LA-8610-MS

1

Oxidation of Depleted Uranium Penetrators and Aerosol Dispersal at High Temperatures

LOS ALAMOS SCIENTIFIC LABORATORY
Post Office Box 1663 Los Alamos, New Mexico 87545

This report was not edited by the Technical Information staff.

This study was conducted on the recommendation of the Joint Technical Coordinating Group for Munitions Effectiveness, Working Group on Depleted Uranium Munitions, and was supported by the Office of the Assistant Project Manager for Tank Main Armament Development, XMI Tank System, under Army Project No. 1L663608D060. The technical monitors were the Working Group Chairman, E. W. Bloore, and E. F. Wilsey, both of the U.S. Army Armament Research and Development Command, Dover, New Jersey.

LA-8610-MS

UC-41
Issued: December 1980

Oxidation of Depleted Uranium Penetrators and Aerosol Dispersal at High Temperatures

J. C. Elder
M. C. Tinkle

CONTENTS

OXIDATION OF DEPLETED URANIUM PENETRATORS AND AEROSOL DISPERSAL AT HIGH TEMPERATURES

by

J. C. Elder and M. C. Tinkle

ABSTRACT

Aerosols dispersed from depleted uranium penetrators exposed to air and air-CO_2 mixtures at temperatures ranging from 500 to 1000°C for 2- or 4-h periods were characterized. These experiments indicated dispersal of low concentrations of aerosols in the respirable size range [typically $<10^{-3}$% of penetrator mass at 223 cm/s (5 mph) windspeed]. Oxidation was maximum at 700°C in air and 800°C in 50% air-50% CO_2, indicating some self-protection developed at higher temperatures. No evidence of self-sustained burning was observed, although complete oxidation can be expected in fires significantly exceeding 4 h, the longest exposure of this series. An outdoor burning experiment using 10 batches of pine wood and paper packing material as fuel caused the highest oxidation rate, probably accelerated by disruption of the oxide layer accompanying broad temperature fluctuation as each fuel batch was added.

I. INTRODUCTION

This report describes a series of experiments requested by the U.S. Army Armament Research and Development Command (ARRADCOM) and performed jointly by Groups H-5 (Industrial Hygiene) and CMB-8 (Physical Chemistry and Metallurgy) of Los Alamos Scientific Laboratory (LASL). The primary purpose of the experiments was to characterize the nature and amount of uranium particles dispersed if depleted uranium (DU) metal penetrators in anti-tank munitions (designated XM774) were subjected to fire in a storage depot or during transport. Normal storage condition for DU munitions is within a large covered bunker (igloo) in the presence of excess air, soft pine wood storage boxes, paper-base packing tubes, and artillery propellant within the shell casings. These materials are all combustible. Uranium is a pyrophoric material but sustains burning only in finely divided form, that is, dispersed small fragments or fine turnings.[1] Since published data were limited on the dispersion of aerosols from large DU metal rods similar to the

penetrators, these experiments were initiated to simulate, in semi-controlled conditions, the exposure of the penetrators to high temperature, oxidizing atmosphere, and an intermediate wind speed of 223 m/s (5 mph).

The first phase of these experiments consisted of three simplified outdoor burn tests in which burning DU turnings or artillery propellant provided the heat source. The second phase consisted of laboratory experiments in which penetrators were exposed to temperatures from 500 to 1000°C (all under the 1132°C theoretical melting point of DU metal) in a tube furnace under dynamic flow conditions of air or an air-CO_2 mixture. The third phase consisted of a prolonged outdoor burn within a wind tunnel apparatus. The heat source was the combustion of soft pine wood and paper packing tube material in a 2.5 to 1 ratio by weight to simulate packing conditions of the XM774 round. The determination of characteristics of DU aerosols under violent conditions such as combined wood fire and rapid propellant burning by which penetrators could be displaced into or out of high temperature regions was considered beyond the scope of this test series.

Coleman and Schwendiman[2] investigated particulate release from 0.69- by 1.9-cm long uranium cylinders at furnace temperatures from 400 to 1200°C. They observed a general increase in oxide particle size with increasing temperature. Less than 4% of the oxide formed was in the <10-μm aerodynamic equivalent diameter (D_{ae}) particle size range in any of the cases they investigated. The air velocities over the cylinders were 8.3, 33.2, and 66.4 cm/s (significantly lower than the 223 cm/s suggested by ARRADCOM for our study). Effect of air velocity on the aerodynamic entrainment of uranium oxide particles was not clearly deduced in the referenced study, although the authors expected air velocity effects to be more significant in entraining the smaller particles formed at lower temperatures (400-800°C). The specimens generally remained intact until significant temperature change occurred to cause flaking during thermal contraction.

In another study, Megaw, et al.[3] oxidized one kilogram uranium slugs at temperatures up to 1000°C in air and pure CO_2. Air velocities ranged from 85 to 260 cm/s. Increasing particle size with increasing temperature was observed, as in the Coleman experiment. Average particle size decreased with increasing velocity, probably indicative of some breaking up of oxide particles by increasing turbulence. In the Megaw experiment, the specimens were heated in a high frequency eddy current furnace rather than by heating coils external to the furnace. A sharp increase in oxidation rate was noted between 750 and 800°C and was attributed to beta-gamma phase transition at 771°C. Slightly higher oxidation rates occurred in pure CO_2 than in air.

II. EXPERIMENTAL APPARATUS AND TECHNIQUES

The XM774 penetrator is shown in Fig. 1. This pointed rod is 34.5-cm long, 2.59-cm nominal diameter, and weighs 3355 ± 3 g. Its surfaces are smooth except for the 12.7-cm section of buttress grooves (2.94-cm maximum diameter, 2.59-cm minimum diameter) located approximately midway and the 2.1-cm threaded length on one end. In its normal storage and deployment configuration, the penetrator is covered by a thin aluminum windscreen and a thicker three-piece aluminum sabot which joins the penetrator to the shell casing and an aluminum tail fin threaded onto the rear of the penetrator. None of the experiments described here employed the aluminum pieces to evaluate the fire protection the aluminum might offer the penetrator. Aluminum melts at approximately 650°C and would only offer protection to a penetrator at the periphery of a fire.

Techniques used to evaluate oxidation and measure particle size characteristics were consistent among the various experiments and are described below. In general, exposure times were selected as follows:

(1) Fuel was expended, concluding the burn test;

(2) 2-h run time was arbitrarily selected in the early laboratory experiments as producing a desired effect on the penetrator; and

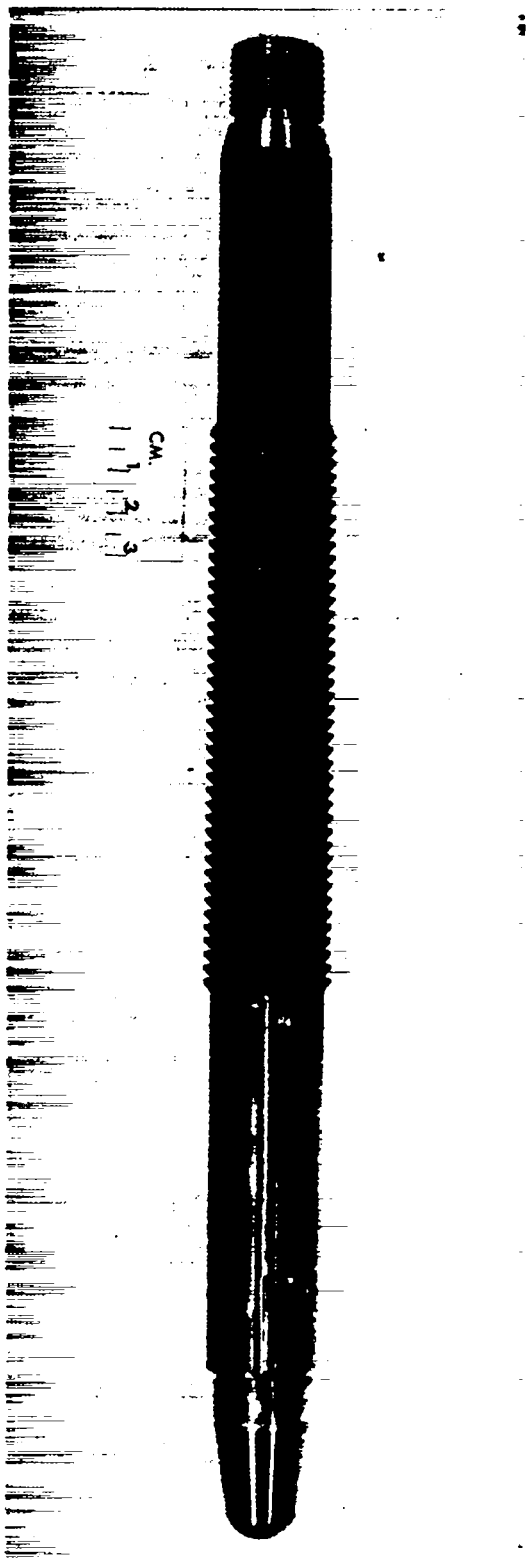

Fig. 1.
Penetrator XM774.

(3) 4-h runs were conducted in the later laboratory runs at DARCOM request.

The 223 cm/s (5 mph) gas velocity was selected as a reasonable compromise between the two extremes of no wind and heavy wind. In all the experiments the 223 cm/s velocity was provided at the plane immediately ahead of the penetrator. In all cases, some change in gas velocity occurred due to the presence of the penetrator and fuel and support structures causing reduced cross-sectional area in the flow channel. These changes were not investigated.

None of the experimental conditions was expected to produce an oxygen-deficient atmosphere. Half of the laboratory experiments were conducted using 50% air-50% CO_2 to simulate an atmosphere containing a combustion product but this was by no means a reducing atmosphere.

A. Analysis Techniques

1. Gravimetric Analysis of Oxidation. Penetrators were cleaned and weighed before each experiment on a Mettler beam balance capable of weighing 4 kg within ±0.1 g. After exposure, each penetrator was cleaned by light mechanical work and motor-driven wire brushing. The penetrator was then weighed on the same balance to determine the oxidation of metal caused by the exposure. Mass balances were performed in the laboratory experiments by separately weighing all oxide removed from the penetrator after the experiment. The penetrator was weighed after the light mechanical work. To account for the nonrecoverable oxide mass removed by brushing, the difference between this prebrushing penetrator weight and the post-brushing penetrator weight was multiplied by a stoichiometric factor of 1.1829 and added to the oxide weight to yield the total oxide mass. The factor of 1.1829 is the theoretical conversion factor for the uranium-titanium alloy reaction to U_3O_8 - TiO_2.

2. High Volume Air Sampling and Analysis. Mass concentration of DU aerosol was determined by mass analysis of samples collected by high volume air samplers with flow rates up to 0.038 m^3/s (80 ft^3/min). These samplers held a glass fiber filter [MSA1106BH (Mine Safety Appliances, Pittsburgh, Pennsylvania)] nominally 20 by 25 cm (8 by 10 in.) and were operated at various flow rates controlled by variable resistor on the blower motor. Gas flow rates were calibrated in advance by pitot tube traverses of the duct. The DU mass collected on each filter was determined by gamma counting one-fourth of the filter with a 10- by 10-cm (4- by 4-in.) thallium-drifted sodium iodide scintillation detector. Minimum detectable level of DU with this counter was 0.040 ± 0.010 mg. Amounts smaller than 0.040 mg were acid leached from the glass fiber filters using an HCl acid leach-ion exchange procedure (with about 40% recovery) and submitted for separate analysis by delayed neutron counting technique.[4] The acid leach removed collected DU and the ion exchange removed sodium which interfered with the delayed neutron counting analysis. Delayed neutron analysis requires the samples to be placed in a 25-cm^3 vial, exposed to a high thermal neutron flux, and counted for delayed neutrons produced from fission of the residual ^{235}U in the DU. Minimum detectable level of DU by this method was 0.02 μg. DU standards were prepared for each set of samples.

The first sets of DU samples (Burns 1, 2, and 3) were not successfully analyzed due to erroneous scaling of DU mass on the first samples. These samples were submitted for analysis by the method routinely used for urinalysis, which was scaled for much lower concentrations, and were disposed of after one count. Thereafter, special analysis procedures were initiated to prevent future mishandling of samples.

3. Aerosol Size Analysis. Particle size characterization obtained during most of the experiments was obtained using one of two configurations of an inertial cascade impactor [Andersen eight-stage ambient sampler with 10-μm D_{ae} precutter (Andersen Samplers, Inc., Atlanta, Georgia)]. Normal impactor sampling flow rate was 28.3 L/min (1 ft^3/min) at ambient conditions (approximately 775 mb and 20°C). Effective cutoff diameters (D_{50}s) for each stage in the two configurations were:

Complete Impactor		Short Impactor	
Stage	**D_{50} (μm)**	**Stage**	**D_{50} (μm)**
Precutter	10	Precutter	10
0	9	0	9
1	5.8	-	-
2	4.7	-	-
3	3.3	-	-
4	2.1	-	-
5	1.1	-	-
6	0.7	-	-
7	0.4	-	-
Backup filter	-	Backup filter	-

The short impactor provided <10-μm information with fewer samples. Stage 0 was included only to provide mechanical transition between the precutter and the backup filter. An 8.2-cm glass fiber backup filter collected all particles passing the impactor stages.

Impactor mass data were analyzed by a computerized least-squares curve fitting routine in which a lognormal distribution of particle aerodynamic diameters was assumed. This distribution is described by two parameters, mass median aerodynamic diameter (mmad) and geometric standard deviation (σ_g). The data analysis technique included only the stage masses (not the precutter mass) owing to the predominance of the precutter mass in most samples. Including the precutter mass as an additional stage of the impactor resulted in mmads larger than 20 μm, which was well beyond the meaningful range of the impactor. Separate reporting of the precutter mass and stage masses was considered more appropriate. Sample substrates covering the impaction plates were membrane filters [Millipore Type AA (Millipore Corporation, Bedford, Massachusetts)] throughout the laboratory experiments and in Burns 1, 2, and 3. Substrates were changed to glass fiber filters on inverted impaction plates to allow for heavier loading in Burn 4.

The effect of gas temperature on impactor calibration was not corrected for, owing to expected difficulty in measuring gas temperature at each impaction stage in each experiment. The maximum error in D_{50} (largest at the precutter and stage 0) would be proportional to $(\text{viscosity})^{1/2}$ where viscosity of air increases from 183 micropoises at 18°C (calibration temperature) to 211 micropoises at 75°C (estimated maximum at Stage 1 during the laboratory experiments). The maximum correction factor applied to the precutter and the first few impactor stages in this case would be approximately 1.07 or <10% error in D_{50}, which is not significant in this instance.

Analysis of mass collected on impactor stages was initiated by screening each sample with the gamma counter. When the deposit was too small for gamma counting analysis, the sample was analyzed by delayed neutron counting, either directly if a membrane filter sample or after acid leaching and ion exchange if a glass fiber sample. Membrane filters were folded and deposited in 25 cm^3 vials for delayed neutron counting analysis described earlier.

4. Particle Sizing by Sieving and Sedimentation. The oxide material collected from the tube furnace in the laboratory experiments was subjected to sieve analysis to separate size fractions down to U.S. Standard No. 400 sieve (38 μm).[5] The below 400-sieve material was then subjected to sedimentation size analysis. The total oxide from each run was first sieved by hand on a U.S. Standard No. 12 sieve to remove very large pieces from the gross powder. Approximately 100 g of the DU oxide passing the No. 12 sieve was weighed to the closest 0.1 g and analyzed in a set of nested sieves of the U.S. Standard series No. 16, 20, 30, 40, 50, 70, 100, 140, 200, 270, and 400. A Tyler (W. S. Tyler, Inc., Mentor, Ohio) Ro-Tap shaker accommodated six standard sieves at a time, requiring two sieve runs for each analysis. The sieving time was 15 min. The mass fractions retained by each sieve were weighed to the nearest 0.1 g and plotted as cumulative percent vs mesh opening on Tyler Screen Scale diagrams. Midpoint (50%) values from these plots provided an indication of central tendency, that is, a mass median diameter of nonairborne particles.

Particles passing through the U.S. Standard No. 400 sieve were submitted for size analysis by the Sartorius Sedibal method.[6] This method records mass increase vs time on a microbalance pan at the bottom of an ethylene glycol column. Oxide particles were prepared for analysis by ultrasonically agitating a suspension of 0.6 g oxide in ethylene glycol for 10 min to separate aggregated particles. The suspension was then introduced into the column and stirred. Mass settling on the microbalance was then recorded over appropriate time intervals. Sedimentation techniques describe the particle size characteristics of the batch powder in terms of Stokes diameter, which is the diameter of a sphere of the given density of the material which, in the same suspension media and force field, has the same terminal settling velocity. Stokes diameter (STK) can be converted to D_{ae}, the diameter of a unit density sphere with the same terminal settling velocity in air, by multiplying by (particle density x slip correction)$^{1/2}$. If the particle size of interest is larger than approximately 1.5-μm geometric diameter, the slip correction is 1.0 and may be neglected in this conversion. As will be noted in describing the sedimentation results later in this report, this conversion was applied to sedimentation results to allow comparison with impactor results.

B. Outdoor Burn Tests

The four burning experiments described in this report were conducted at R-Site, Los Alamos Scientific Laboratory, an unforested area used extensively over the past 25 years for experiments involving uranium. Background uranium was a potential problem in the first three burning experiments due to their proximity to heavy soil contamination at firing points E-F. This experience prompted moving the Burn 4 apparatus to a paved, low background area nearby.

Burns 1, 2, and 3 were simple preliminary experiments to determine if the penetrators could be ignited. The penetrators were exposed to heat under expeditious, yet descriptive conditions of oxidation in excess air. Figure 2 summarizes the conditions and general configuration of each burn test. Figures 3 and 4 show the arrangement of the Burn 2 apparatus, which differed from Burn 1 and 3 only in the airflow path through the fuel-penetrator stack. All effluent gas from the hood in Burns 1 and 2 passed through the high volume air sampler. Burn 3 permitted open burning of the propellant followed promptly by placement of hood and samplers. Burn 4 permitted release of the smoke plume to the atmosphere. Occasional samples of Burn 4 effluent taken isokinetically with gross filter and eight-stage impactor with precutter collected aerosol for particle size characterization.

Thermocouples were added to measure penetrator temperatures after Burn 1. Chromel-alumel thermocouples were installed on the Burn 2 and 3 apparatus. Temperatures of the Burn 4 penetrators were monitored by platinum-platinum-rhodium thermocouples attached to each penetrator. Each new batch of wood-paper fuel (10 total) was added to the furnace through a side

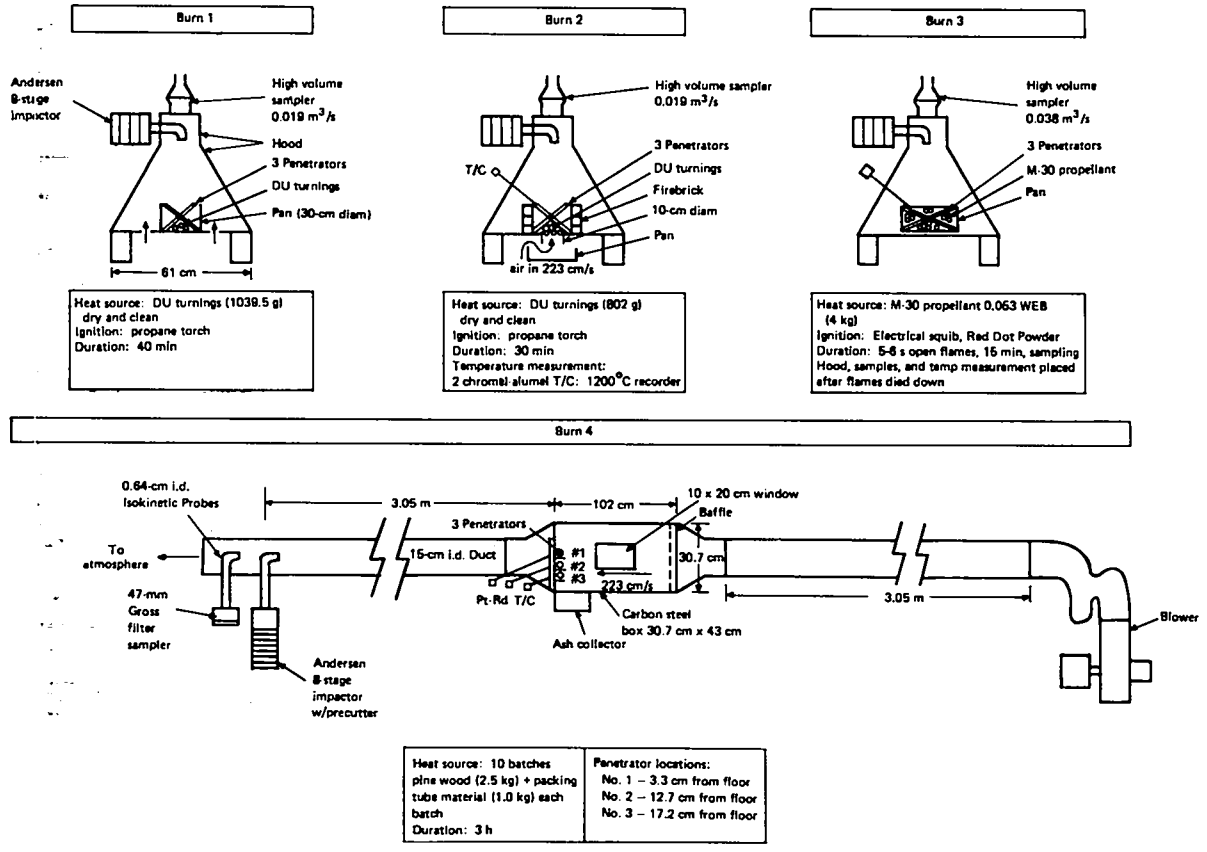

Fig. 2.
Summary of outdoor burning experiments, general layout.

port. The side port was normally closed by a Pyrex glass window which allowed observation of the fire. A view of the penetrators and furnace configuration is presented in Fig. 5.

C. Laboratory Oxidation and Aerosol Experiments

The laboratory experiments were conducted at Wing 4, basement of the CMR Building, Los Alamos Scientific Laboratory. Production of uranium compounds and other activities involving uranium are routinely performed in this laboratory.

Arrangement of the tube furnace and air samplers used in the laboratory experiments is shown in Fig. 6. The tube furnace was a quartz tube 90-mm i.d. and 122 cm in length. Each penetrator was located on the center line of the tube and was centered in the heat zone of the nichrome wire furnace. The penetrator was supported on two lavite (soap stone) pedestals that were 1.3-cm wide, approximately 23 cm apart, and contacted the penetrator over a 120°arc. The pedestals were perforated with large holes to permit gas flow on the underside of the penetrator; however, some obstruction of gas flow probably occurred. A smaller support was located midway between the larger supports to limit sag of the penetrator at the higher temperatures.

The nose of the penetrator was usually pointed into the flow of gas; however, during the first three experiments the penetrator was positioned with the blunt end pointing into the gas stream to allow insertion of a thermocouple (T/C 2) into the 3-mm-diam hole at the blunt end of the

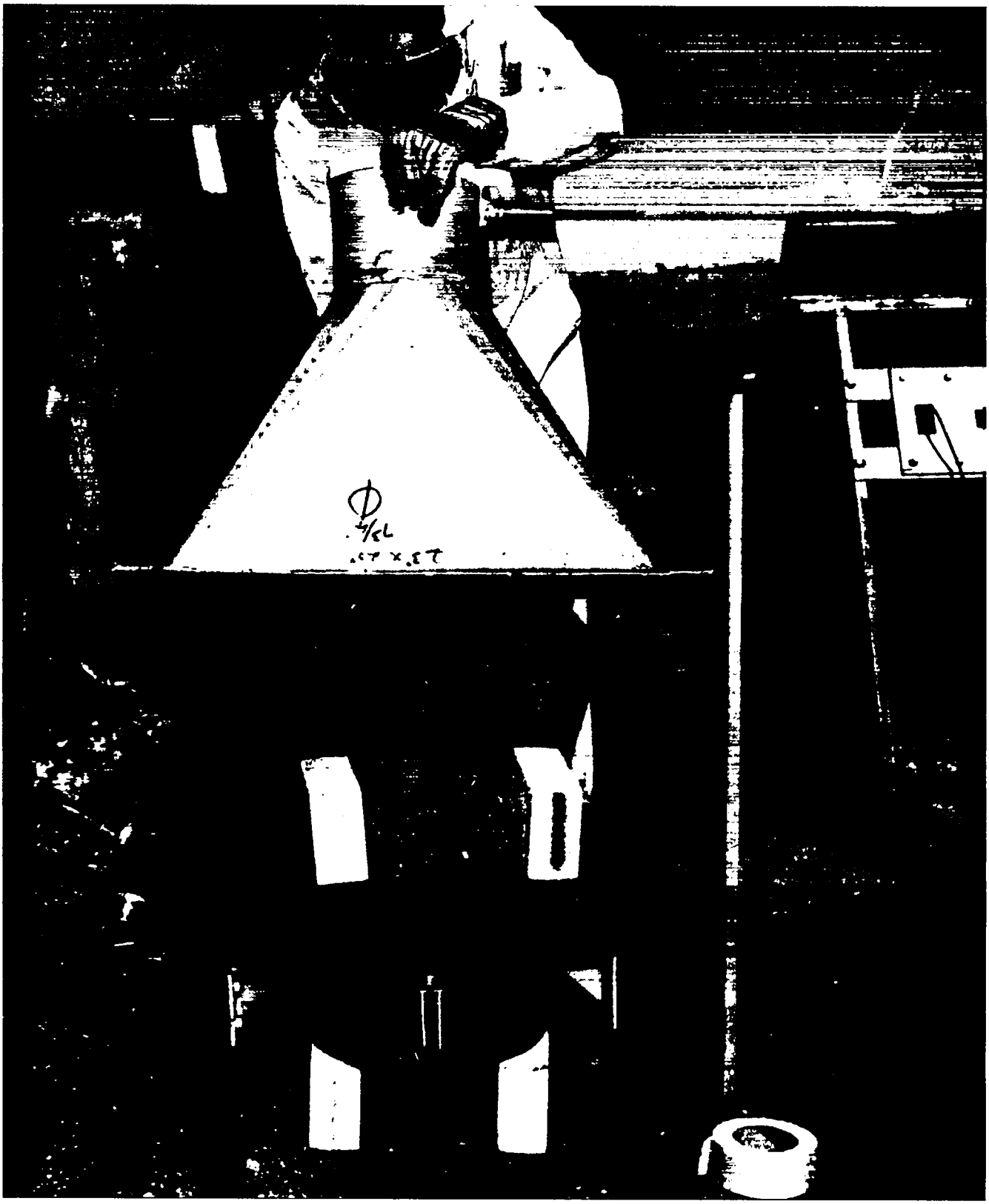

Fig. 3.
Burn 2 apparatus before assembly.

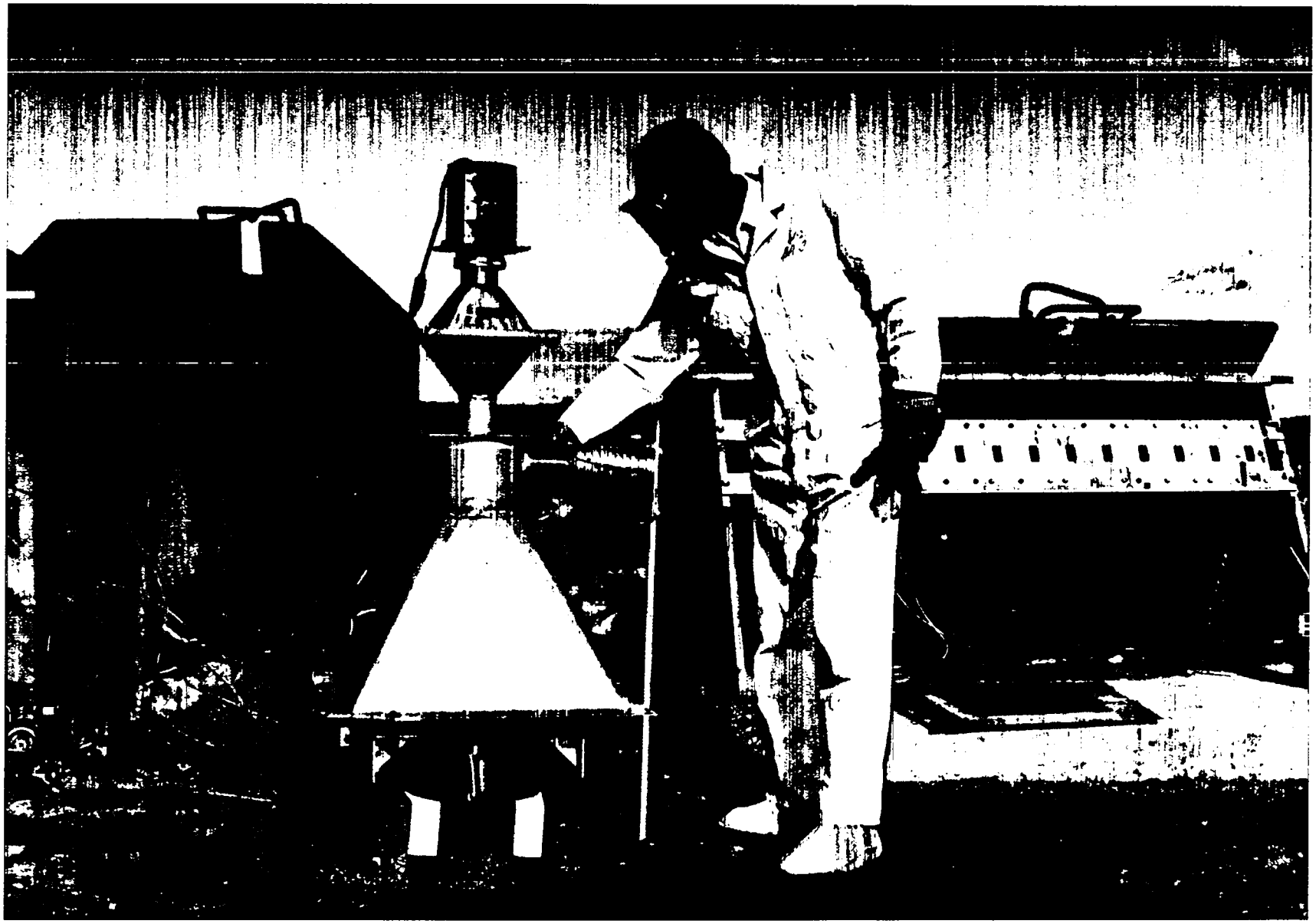

Fig. 4.
Burn 2 apparatus fully assembled.

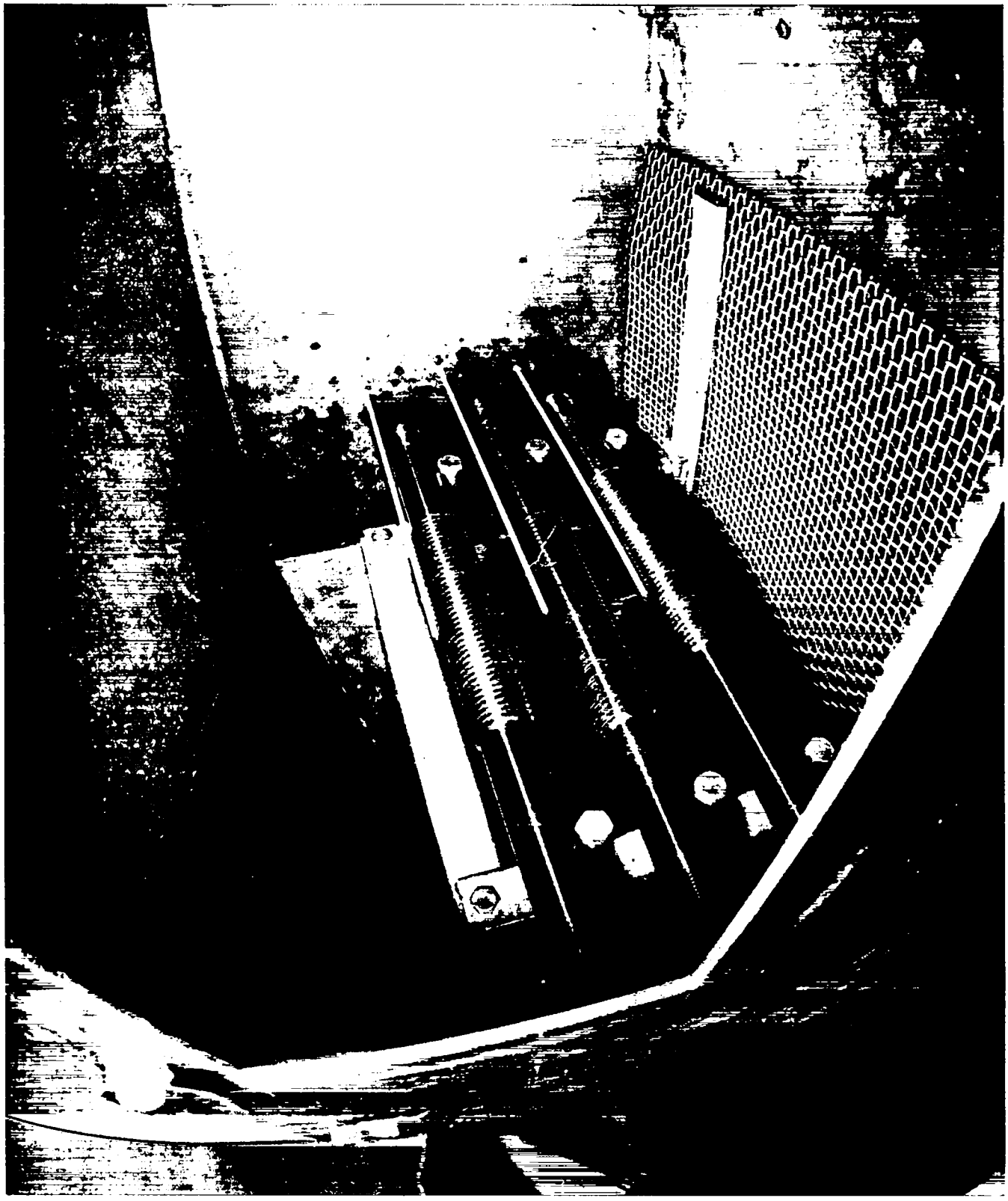

Fig. 5.
Interior setup of Burn 4 furnace box.

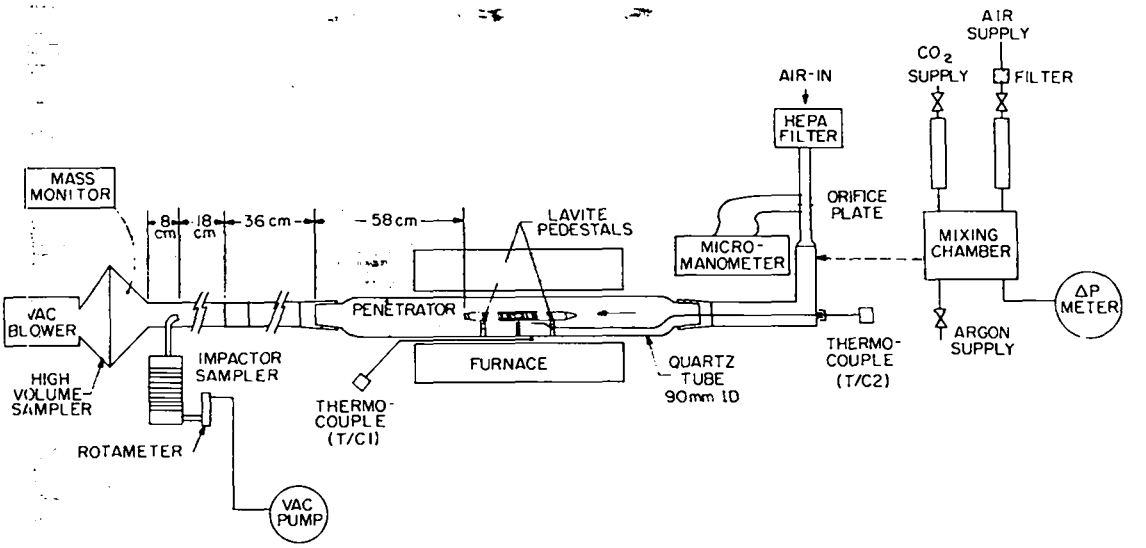

Fig. 6.
Laboratory experimental apparatus.

penetrator. When this proved unsatisfactory, the thermocouple was placed alongside the penetrator and the penetrator was reversed to direct its nose into the gas flow. Thermocouple T/C 2 was placed in contact with the penetrator approximately 2.5 cm downstream of the first buttress groove. T/C 2 provided consistent indication early in the run but drifted later as oxide began to form on the penetrator, changing airflow around the thermocouple, or as the oxide sloughed off the penetrator, leaving the thermocouple more exposed to cooling. Therefore, data from T/C 2 during its stable period was used to determine the desired "nominal" temperature at its position; thereafter, T/C 1 controlled furnace temperature at the nominal temperature. Since incoming gas cooled the upstream end of the penetrator and caused a temperature gradient along its length, the nominal temperature should be considered an average temperature approximately 15 cm from the upstream end of the penetrator. Although total temperature gradient along the penetrator was not measured, it probably was as high as 100°C in the high temperature runs.

In all experimental runs using air as the oxidizing gas, room air was drawn through a high-efficiency particulate air (HEPA) filter before entering the system. Airflow rate was determined by measuring the differential pressure across a calibrated sharp-edged orifice using a micromanometer. Gas flow of the air-CO_2 mixtures was measured by rotameters calibrated against a dry test meter. The gas mixture was based on equal volumes of CO_2 added from gas cylinders and filtered air added from the building compressed air system. These gas streams were mixed in a chamber and allowed to equilibrate at room temperature before being introduced into the tube furnace. Oxidation of the penetrator during heating and cooling periods was retarded by purging the tube furnace with argon gas.

A sample of the aerosol entrained in the gas stream downstream of the penetrator was collected by an eight-stage Andersen impactor for particle size analysis. The remainder of the gas flow passed through a high volume sampler that provided primary suction for the test system. Flow through the high volume sampler ranged from 147 ambient L/min at test conditions of 1000°C in the tube furnace to 242 ambient L/min at 500°C.

Air samples from each run submitted for DU mass analysis consisted of a glass fiber filter carrying the contents of the precutter; eight Millipore filter impactor stage substrates; the glass fiber backup filter; a 10- by 12-cm glass fiber filter used to swipe the inlet tube to the high volume sampler; a similar swipe of the high volume sampler holder; and four quarters of the 20- by 25-cm high volume sampler filter.

A GCA portable respirable mass monitor (GCA/Technology Division, Bedford, Massachusetts) Model 101-1, was connected by flexible tube to the high volume filter holder on 12 of 15 experimental runs to detect the time of onset of aerosol production. Sampling flow rate for this instrument was only 2 ambient L/min, not enough to interfere with the high volume sample. Sensitivity of the instrument was approximately 0.1 mg/m^3. Only a qualitative indication of the presence of aerosol was expected from this instrument.

III. RESULTS AND DISCUSSION

A. Outdoor Burn Tests

1. Burn 1, 2, and 3. Gravimetric analysis results of these preliminary burn tests are listed in Table I. Aerosol size characteristics data were not successfully obtained in these tests. Exposure of three penetrators to heat from burning uranium turnings in still air (Burn 1) caused negligible weight change or visually detectable surface change. Uranium from the turnings was recovered within 0.5 g. The presence of aerosol was indicated only by light discoloration of the high volume sample.

Burn 2 results showed significant mass loss from all three penetrators (total 71.0 g). The forced draft condition apparently caused significantly higher local heating. Although full time temperature measurements were attempted, thermocouples at the center of the DU turnings bundle went off-scale at 1200°C within 5 s of ignition and remained off-scale until 5 min, 15 s into the burn. The 347 stainless steel sheath of one thermocouple melted near its tip; this metal melts at 1400-1425°C. Two of the three penetrators were slightly bent, indicating that some softening occurred. The melting point of pure uranium is 1132°C, which is below the estimated maximum temperature for this run. However, the massive size of the penetrators and the lack of uniform heating over their full length probably prevented general melting.

Burn 3 demonstrated that exposure of penetrators to a short, but intense fire did not have a significant effect as indicated by an observable surface change. Thermocouples and air samplers placed over the fire pan after propellant burnout indicated low temperature (approximately 100°C) 1 min after the propellant burn and little aerosol as indicated by slight discoloration of the high volume sample. This test might have been more descriptive if thermocouples of adequate range (>1200°C) had been located in the propellant during the burn.

The general results of Burns 1, 2, and 3 showed (1) self-sustained burning of the penetrators did not occur, (2) oxidation of the penetrators occurred only in the forced-draft case (Burn 2), and (3) airborne material was produced in Burn 2.

2. Burn 4. The results of Burns 1, 2, and 3 led to further investigation of the forced-draft case in Burn 4. Direct exposure to the packing material fire, fanned by a 223 cm/s (5 mph) wind for 3 h was expected to represent a severe exposure condition. Since conditions of time, temperature, and wind velocity in a storage fire have not been postulated, it can only be surmised that these test conditions equaled or exceeded those of a storage fire.

Temperature cycles between each of 10 batches of fuel ranged from 700 to 900°C (see chart records in Addendum A). T/C No. 1 on the bottom penetrator was broken during installation and exhibited erratic performance. Highest temperatures were noted at the top penetrator (No. 3); 1100°C was exceeded during burning of 4 of the 10 batches.

Final penetrator weights after approximately 3 h exposure in the furnace box are shown in Table II. The middle penetrator was oxidized the most (47%). The least oxidation occurred at the bottom penetrator (42%), which was probably shielded somewhat by the ashes collected in the

TABLE I

BURN 1, 2, AND 3

Gravimetric Results

Burn No.	Penetrator Serial No.	Mass Before Test (g)	Mass After Test (g)	Gain or Loss (g)
1	F059609	3354.0	3354.1[a]	+0.1
1	F059201	3355.6	3355.8[a]	+0.2
1	F045305	3354.0	3354.1[a]	+0.1
2	F059609	3354.1	3342.7[a]	-11.4
2	F059201	3355.8	3336.2[a]	-19.6
2	F045305	3354.1	3313.3[a]	-40.8
3	F045207	3357.8	3357.9[b]	+0.1
3	F045221	3353.5	3353.8[b]	+0.3
3	F045501	3356.7	3356.8[b]	+0.1

[a]After cleaning to bare metal.

[b]After scrubbing with water to remove 2-3 g propellant residue.

TABLE II

BURN 4

Final Penetrator Weights

Location	Number	Serial Number	Final Weight (g)	% Oxide (% of Original 3355 g Weight)
Top	3	045313	1874	44
Middle	2	045109	1772	47
Bottom	1	045108	1947	42

bottom of the box. These penetrators are shown in Fig. 7 with the oxide layers still intact after exposure. After removal from the furnace box the penetrators continued to oxidize as they cooled, as shown in Fig. 8. The penetrators were cleaned by wire brushing to remove all oxidized material, as shown in Fig. 9. Each sagged noticeably between the two supports of the frame.

The relatively high loss of material from the penetrators in this 3-h burn, 45% vs 25% on the average in the 4-h lab runs (700°C and above from Table IV) probably resulted from rapid temperature fluctuations causing the protective oxide layer to break away and expose fresh metal surface to be oxidized.

Air sampling results from Burn 4 are summarized in Table III. Oxide mass concentrations in the tailpipe effluent ranged from 4.2 mg/m^3 during Batch 1 to 782 mg/m^3 during Batch 8. These air samples were initiated after the new batch of fuel was actively rekindled (4 to 5 min after restart of the blower). Variation of mass concentration among the four samples is probably attributable to temperature cycles of 700-900°C in progress during the 5-min sampling periods. Differential thermal expansion of the base metal with respect to the oxide layer could cause material to be dispersed, much of it small enough to remain airborne along the tailpipe. The air sampling periods were selected during periods when this material dispersal was probably maximum. Concentrations as high as 782 mg/m^3 (plus some wood smoke) should have been visually detected as a plume. However, visible smoke occurred only briefly upon restart of the blower, a time when the samplers were not operating.

The weight percent associated with particles <10 μm listed in Table III ranged from 20 to 62%. This indicates a high fraction of aerosol mass was in the size range where lung deposition can occur. The 20% <10-μm mass result obtained during Batch 4 was the only sample obtained with all stages in the impactor and appears artifically low with respect to the other three results. Since flow calibrations were made for both impactor configurations and the proper flow rates presumably used, this difference cannot be readily explained. If the same higher flow setting had been erroneously used for all runs, the precutter-backup filter configuration of Batches 1, 8, and 10 would have sampled at 32.4 L/min rather than 28 L/min, causing a sample volume 16% higher than expected and a precutter cutpoint shift downward of <1 μm. This possible error is not large enough to account for the much wider discrepancy in the weight percent <10 μm from Batch 4.

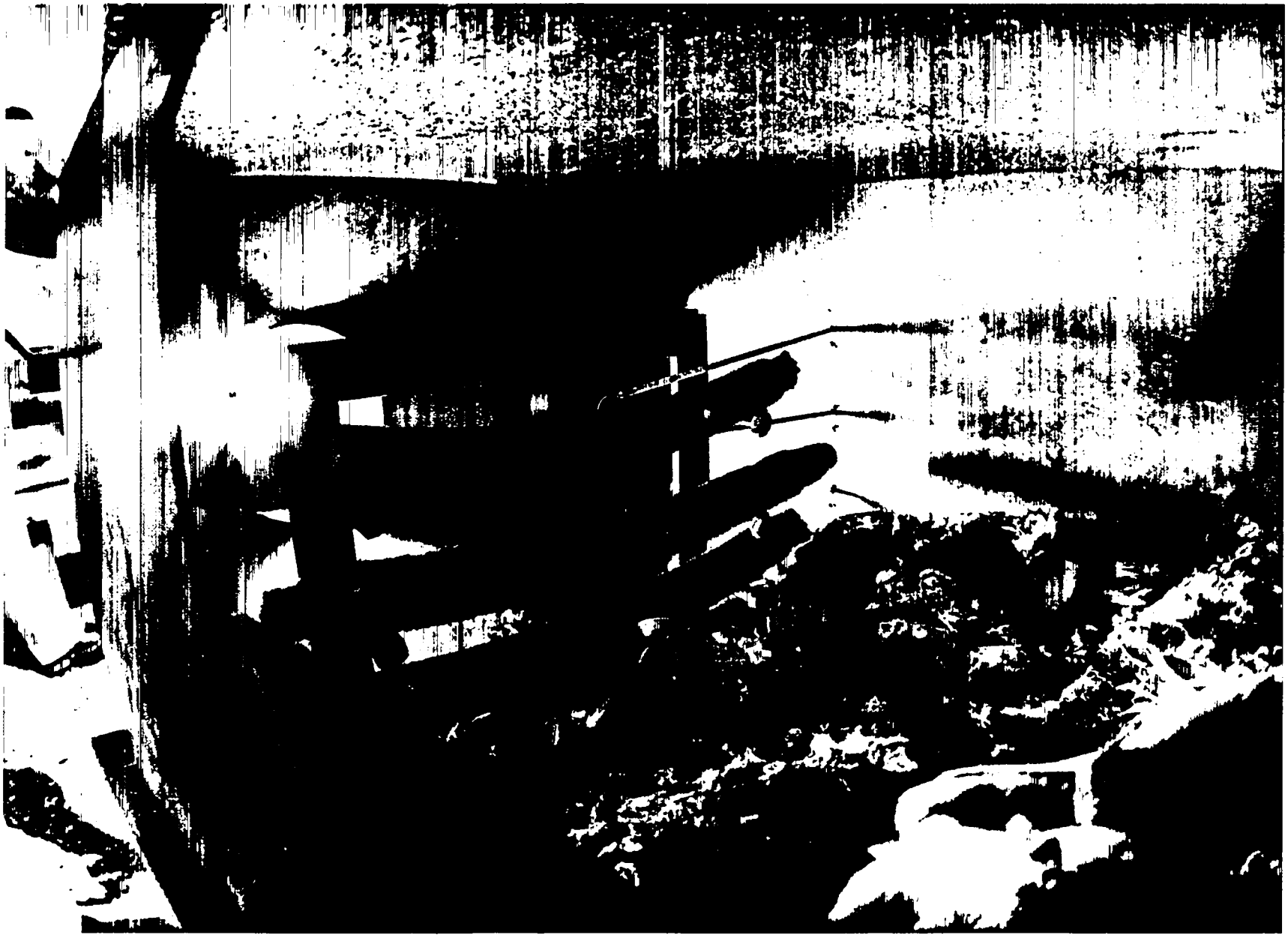

Fig. 7.
Penetrators and debris after Burn 4.

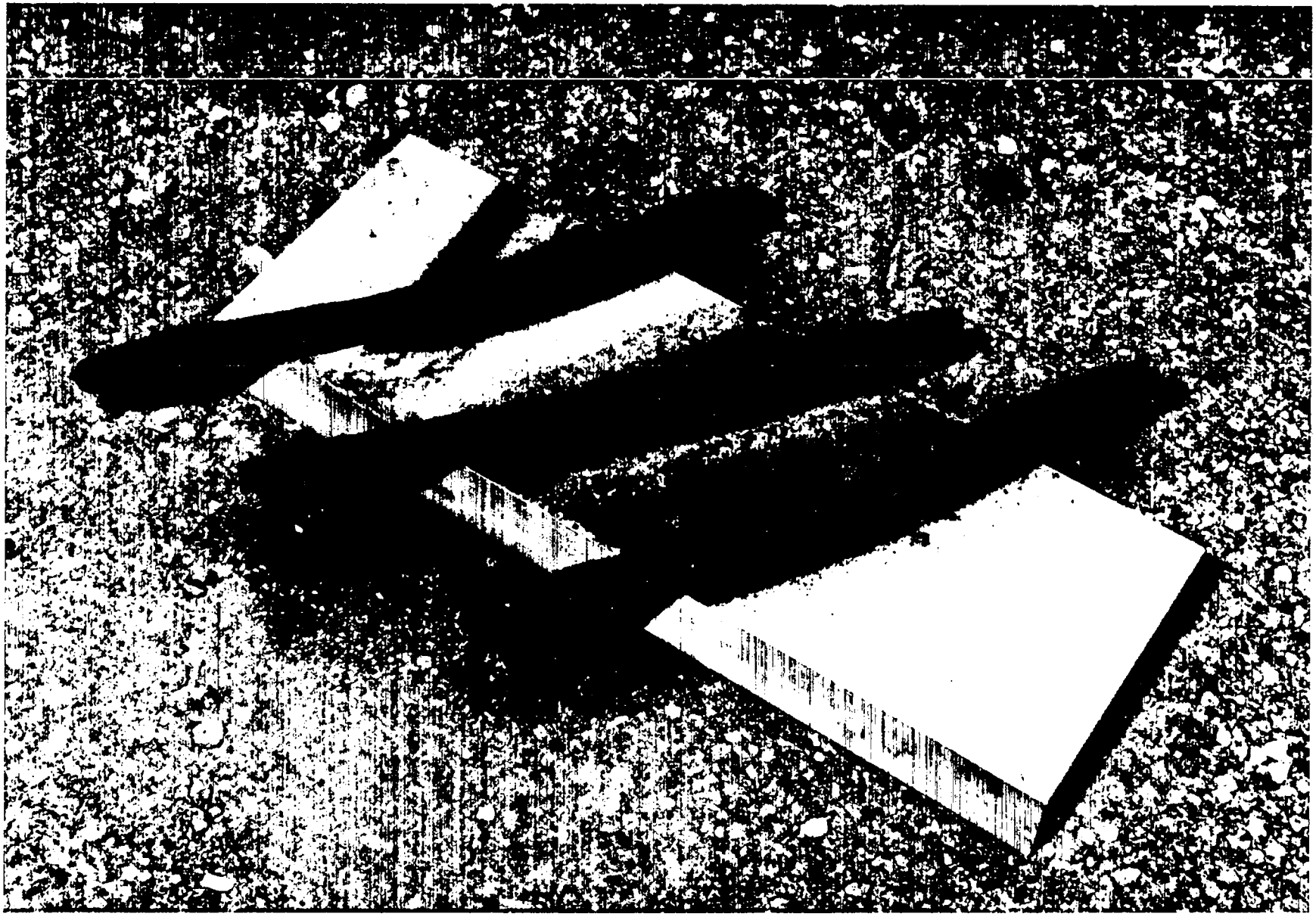

Fig. 8.

Burn 4 penetrators after removal, during cooldown.

Fig. 9.

Burn 4 penetrators after cleaning by wire brushing.

TABLE III

BURN 4 AIR SAMPLING MASSES

Sample	Batch 1	Batch 4	Batch 8	Batch 10
Gross (47 mm) (μg)	931	15062	109407	45749
Andersen Impactor				
Precutter (μg)	482	5695	13998	14980
Stage 0 (μg)	a	1042[b]	a	a
Stage 1 (μg)	a	58[b]	a	a
Stage 2 (μg)	a	34[b]	a	a
Stage 3 (μg)	a	9.8[b]	a	a
Stage 4 (μg)	a	13.5[b]	a	a
Stage 5 (μg)	a	4.5[b]	a	a
Stage 6 (μg)	a	5.9[b]	a	a
Stage 7 (μg)	a	5.4[b]	a	a
Backup Filter (μg)	489	270[b]	21995	24408
Impactor Total[c] (μg)	971	7138	35993	39388
Percent <10 μm[d]	50	20	61	62
Sampling Time (min)[e]	8	5	5	5
Sampling Rate (L/min)	28	28	28	28
Duct DU Mass Conc (mg/m^3)[f]	4.2	108	782	327

[a]Sample not taken (short impactor used).

[b]Particle size characteristics could not be analyzed from these data due to preponderance of mass on Stage 0.

[c]Includes mass collected by precutter.

[d]Percent <10 μm = $\frac{\text{Impactor Total} - \text{Precutter}}{\text{Impactor Total}} \times 100$.

[e]Same sample rate for impactor and gross sampler.

[f]Calculated from gross 47-mm sampler mass. Mass concentration based on the sum of nine masses on impactor stages is not considered as reliable as a single mass on the gross filter.

TABLE IV

PENETRATOR OXIDATION

Run No.	Date	Nominal Temp (°C)	Time (h)	Penetrator No.	Penetrator Weights: Original (g)	Penetrator Weights: After Light Mechanical Removal (g)	Penetrator Weights: After Wire Brush (g)	Metal Oxidation (g)	Metal Oxidation (%)
Air at 223 cm/s									
A-774-7	05-22-79	500	2	61512	3354.0	3130.8	3123.8	230.2	6.8
A-774-2	05-04-79	600	2	59603	3358.8	3162.0	3149.2	209.6	6.2
A-774-4	05-11-79	700	2	61310	3354.9	2640.0	2613.1	741.8	22.1
A-774-6	05-17-79	800	2	61501	3354.5	2794.5	2761.5	593.0	17.6
A-774-5	05-15-79	900	2	61510	3354.0	2869.4	2827.1	526.9	15.7
CO_2-Air Mixture at 223 cm/s									
M-774-1	05-24-79	500	2	61402	3355.0	3156.8	3153.2	201.8	6.0
M-774-2	05-29-79	600	2	61406	3353.0	3149.0	3140.9	212.1	6.3
M-774-3	05-31-79	700	4	45401	3357.0	2652.9	2642.2	714.8	21.3
M-774-5	06-07-79	800	4	45510	3354.2	2405.9	2351.1	1003.1	29.9
M-774-8	07-27-79	800	4	45104	3355.4	2378.1	2343.7	1011.7	30.2
M-774-6	06-12-79	900	4	59613	3352.8	2544.2	2518.8	834.0	24.9
M-774-7	06-19-79	1000	4	45204	3355.0	2586.2	2564.7	790.3	23.6
Air at Zero Velocity									
N-774-1	06-14-79	700	2	45407	3355.9	2929.0	2908.9	447.0	13.3

B. Laboratory Oxidation and Aerosol Experiments

This series of experiments examined the effect of high temperature exposure of bare penetrators under various conditions of air-only and 50% air-50% CO_2 atmosphere at 223 cm/s velocity and zero velocity over time intervals of 2 or 4 h. General results of these experiments indicated (1) absence of self-sustained oxidation of the penetrators after external heat was removed; (2) major effect of temperature fluctuation on the production of aerosol; and (3) production of aerosol in the respirable size range.

At the end of runs with as-planned temperature histories, substantial amounts of fine black oxide (U_3O_8) were noted on the bottom of the furnace tube and all penetrators were coated with an apparently intact layer of black oxide. Only during the cool down period under inert atmosphere did large portions of the oxide layer spall off due to thermal stress. Since this occurred after samplers were stopped, it is unknown if large amounts of this layered oxide was dispersed as an aerosol during the cool down period.

1. Penetrator Oxidation by Mass Loss. Penetrator to oxidation in the 13 experimental runs of the laboratory series are summarized in Table IV. Three other runs, excluded from Table IV due to abnormal temperature fluctuations during the runs, are discussed separately in a later section. Figure 10 shows amount of DU metal oxide after the high temperature exposures. Light mechanical work and wire brushing was used to remove the oxide. Maximum oxidation in air occurred at 700°C (22.1% in 2 h) and in the air-CO_2 mixture at 800°C (30.2% in 4 h). At 500 and 600°C, oxidation was approximately equal for the 2-h runs for both air and air-CO_2. At 800 and 900°C, the effect of extending the exposure time from 2 to 4 h was apparent; doubling the exposure time caused oxidation to increase by a factor of 1.6 to 1.7. The gas mixture had a minor effect on oxidation rate at 500 and 600°C. This is not clearcut at 700°C, where the mass oxidized in air equaled the mass in air-CO_2 in only half the exposure time. On the possibility that this disparity was caused by chemical or heat treatment dissimilarity in the penetrator material, the manufacturer was provided serial numbers for review of chemical analysis. No significant difference was apparent in either the chemical analysis or the heat treatment of the two batches.

Megaw[3] noted a sharp increase in oxidation rate between 750 and 850°C in both air and pure CO_2. The general shape of the temperature vs oxidized metal relationship corresponds to Megaw's results. These results could have been compared more closely if tests at narrower temperature intervals had provided more detail in the vicinity of the phase transition temperature. A decrease in

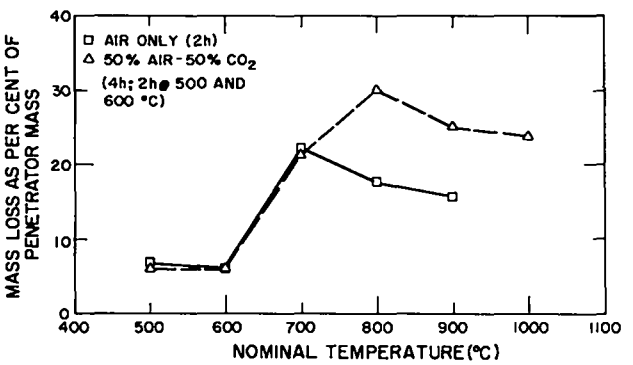

Fig. 10.
Oxidation as a function of temperature.

oxidation at higher temperatures indicated (1) a degree of self-protection occurred as a harder oxide layer formed or (2) the gamma phase was not as susceptible to oxidation as the alpha phase, as suggested by Megaw.[3]

2. Penetrator and Oxide Description. Photographs of penetrators and oxide samples after exposure and cleaning were delivered to ARRADCOM as part of the experimental documentation. The photographs included with the following descriptions were selected as typical or most descriptive of significant results. Unless noted otherwise, the physical appearance of a penetrator exposed to air-CO_2 mixture was the same as the penetrator exposed to air at the same temperature.

***Exposure at 500°C* (2 h).** The sharp edges of the buttress grooves and threads were oxidized and surfaces roughened by a 2-h exposure at 500°C. The oxide came off in long fragile, black layered fragments, some as long as 10 cm (Fig. 11). Round disks of oxide with holes in the center came from the blunt end of the penetrator, which had a 0.32-cm hole in it.

***Exposure at 600°C* (2 h).** Buttress grooves were oxidized but were still visible after 2-h exposure at 600°C. The oxide came off in long black layered fragments, which were more resistant to breakage than the 500°C oxide as shown in Fig. 12.

***Exposure at 700°C* (2 h).** The penetrator exposed to air at 700°C for 2 h is shown in Fig. 13a. The buttress grooves were completely oxidized and deep imprints appeared where the lavite supports conducted heat from the furnace to the penetrator. The effect of temperature gradient along the penetrator was also apparent with only minimal metal oxidation occurring at the blunt end. The black oxide contained fewer large fragments and was broken easily into small pieces as shown in Fig. 14.

The effect of air velocity on the oxidation of DU was investigated in one air run at 700°C with no flow. The penetrator experienced much lower oxidation (447 g vs 742 g) under no-flow conditions. Difference in the oxides of the two cases could not be visually detected.

***Exposure at 800°C* (2 and 4 h).** Sagging of the penetrator was apparent at 800°C, particularly after 4-h exposure (Figs. 13b and 15a). Large pits appeared in the surface over the full length, which was distinctive of this temperature. The black oxides were similar in the 2-h air run (Fig. 16) and the 4-h air-CO_2 run (Fig. 17), being composed of smaller particles and a few intermediate-size fragments.

***Exposure at 900°C* (2 and 4 h).** The penetrators exposed to 900°C appeared in better condition than the penetrator exposed at 700 and 800°C (Figs. 13c and 15b). Remnants of buttress grooves were apparent after 2-h exposure in air. Large pits appeared in the cooler portion of the penetrator exposed for 4 h. The trailing end showed hard, shiny surfaces after wire brushing. The black oxide from the 4 h air-CO_2 run was composed of larger, generally hard, shiny, and dense fragments (Fig. 18), compared to somewhat finer particles from the 2-h run shown in Fig. 19.

***Exposure at 1000°C* (4 h).** The penetrator exposed to 1000°C for 4 h (Fig. 15c) was quite similar to the 900°C penetrator, except for slightly more evidence of buttress grooves. The bulk of its black oxide was also composed of large, hard, dense fragments (Fig. 20).

3. Aerosol Sizing Results. Aerosol size expressed as mass median aerodynamic diameter (mmad) of particles passing the precutter is displayed as a function of temperature in Fig. 21. Geometric standard deviation (σ_g) of these aerosols ranged from 1.7 to 3.6 and indicated a

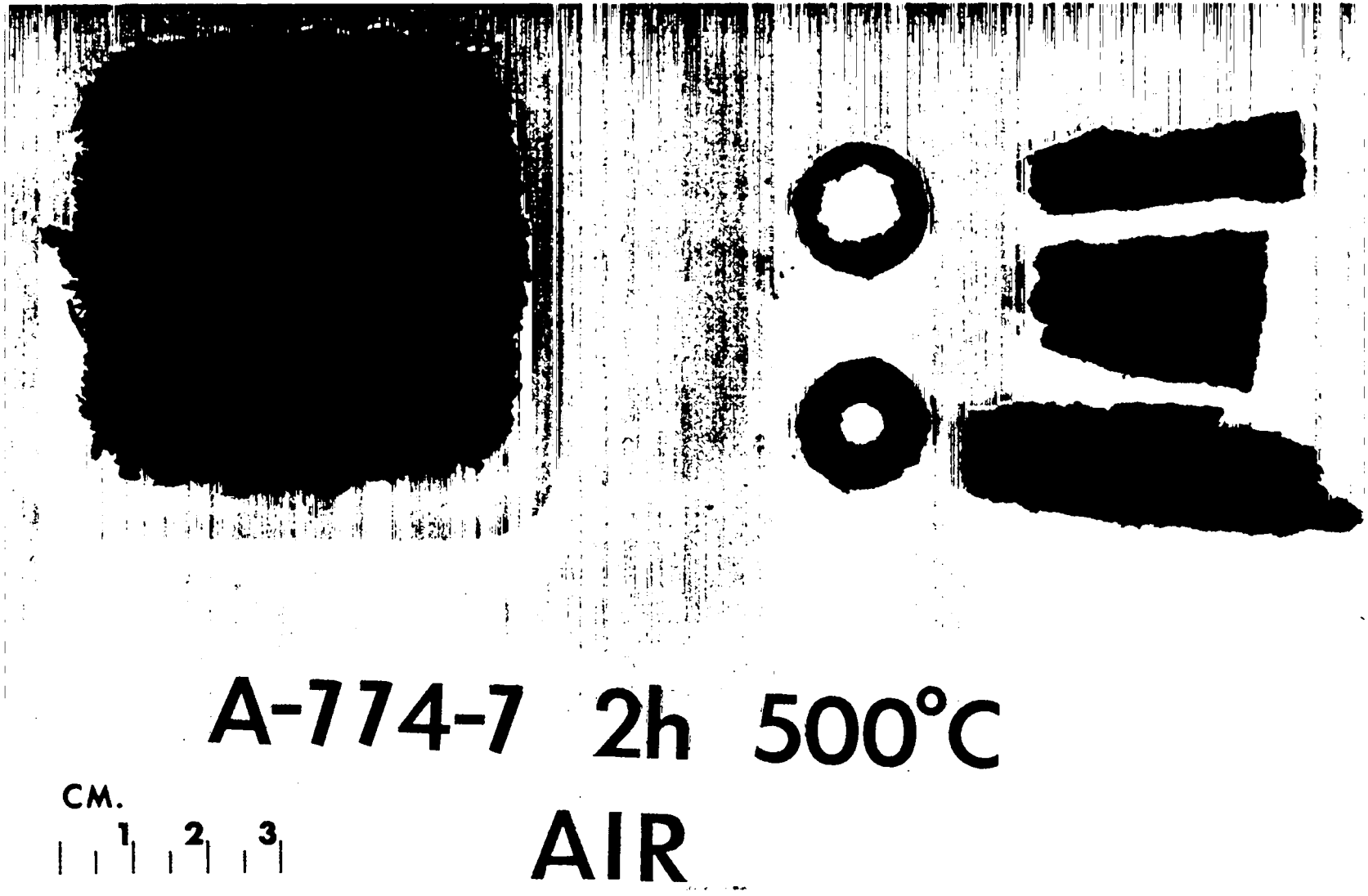

Fig. 11.

Oxide from 500°C air run.

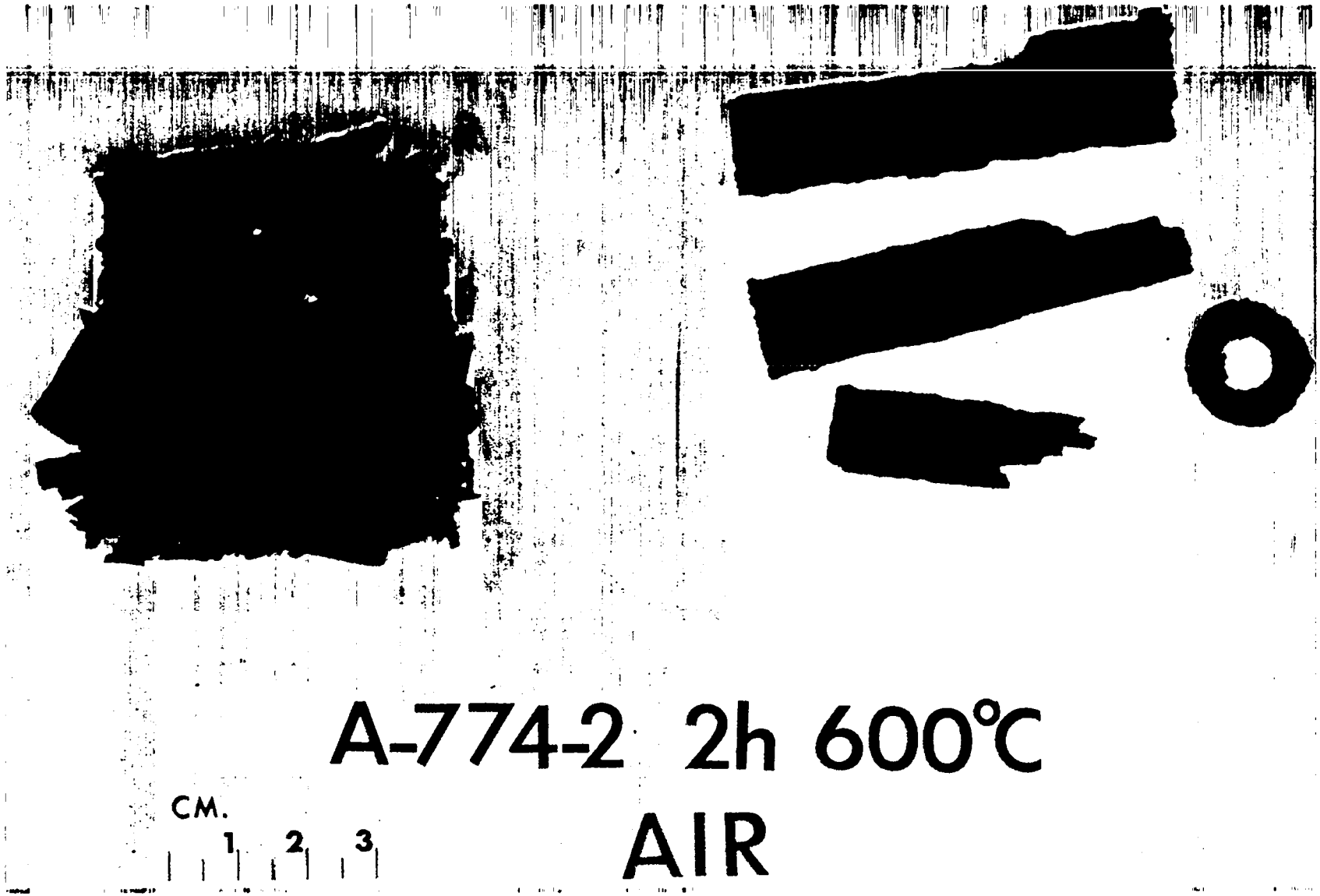

Fig. 12.

Oxide from 600°C air run.

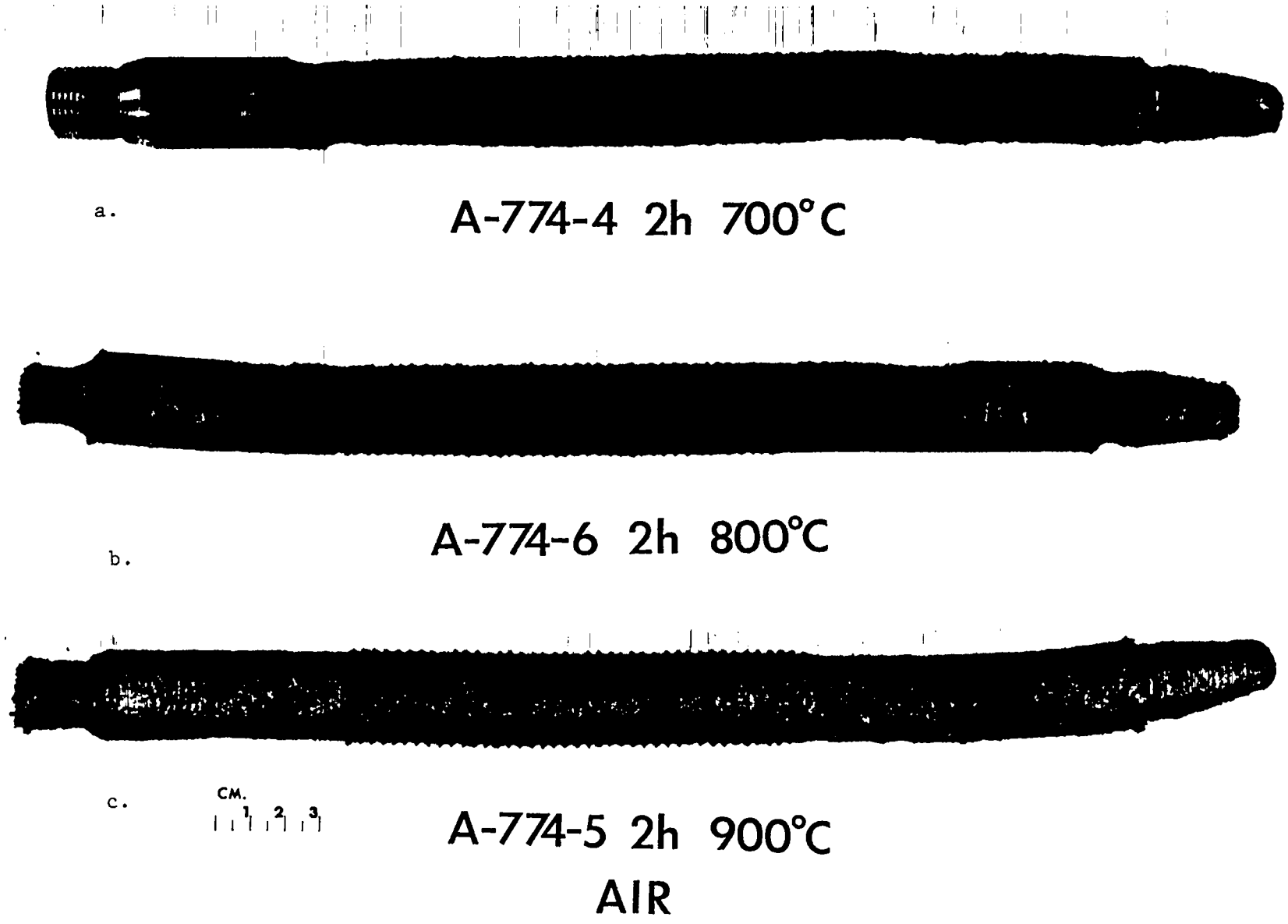

Fig. 13.
Penetrators after exposure to air at the listed temperatures.

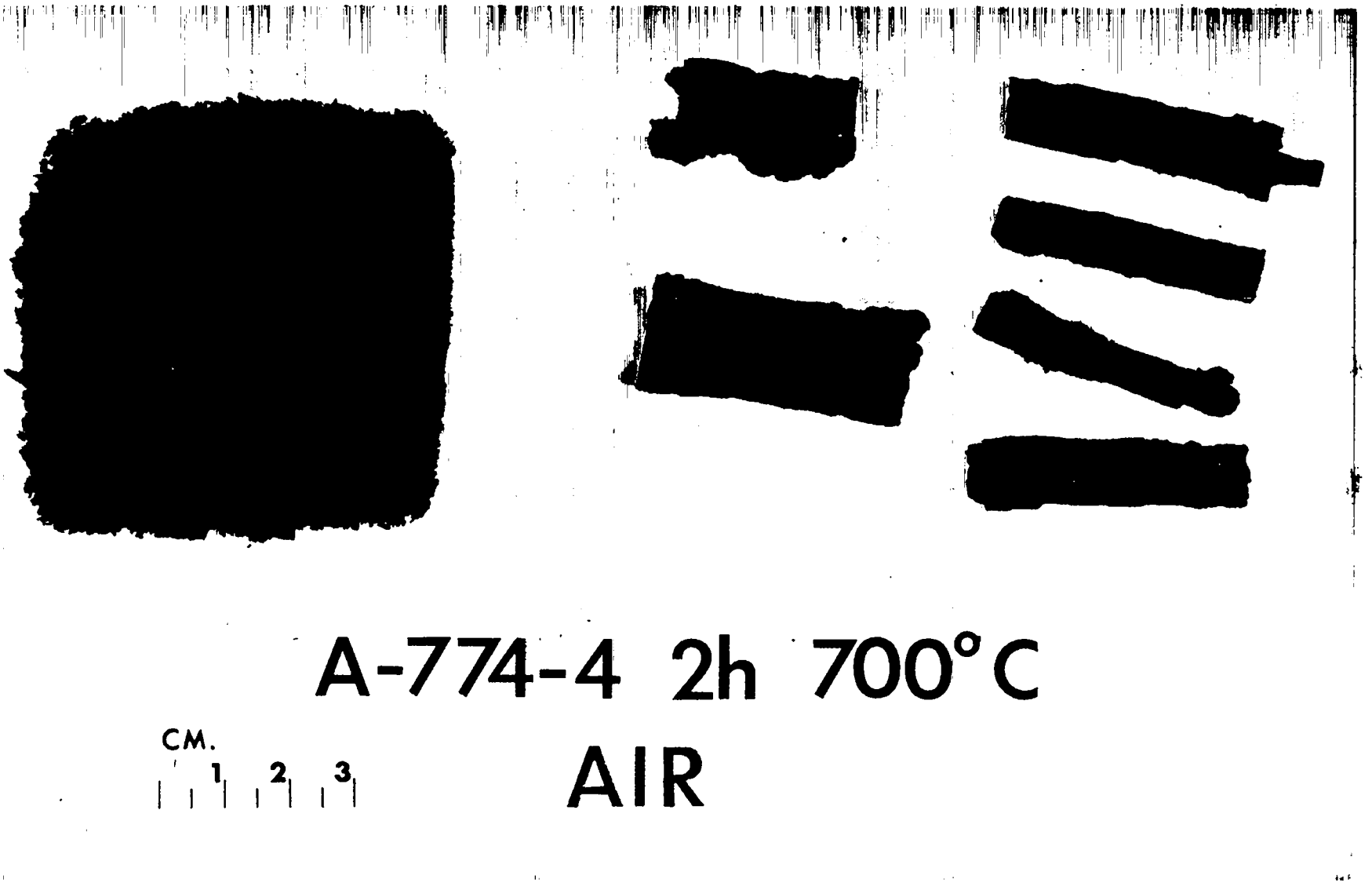

Fig. 14.
Oxide from 700°C air run.

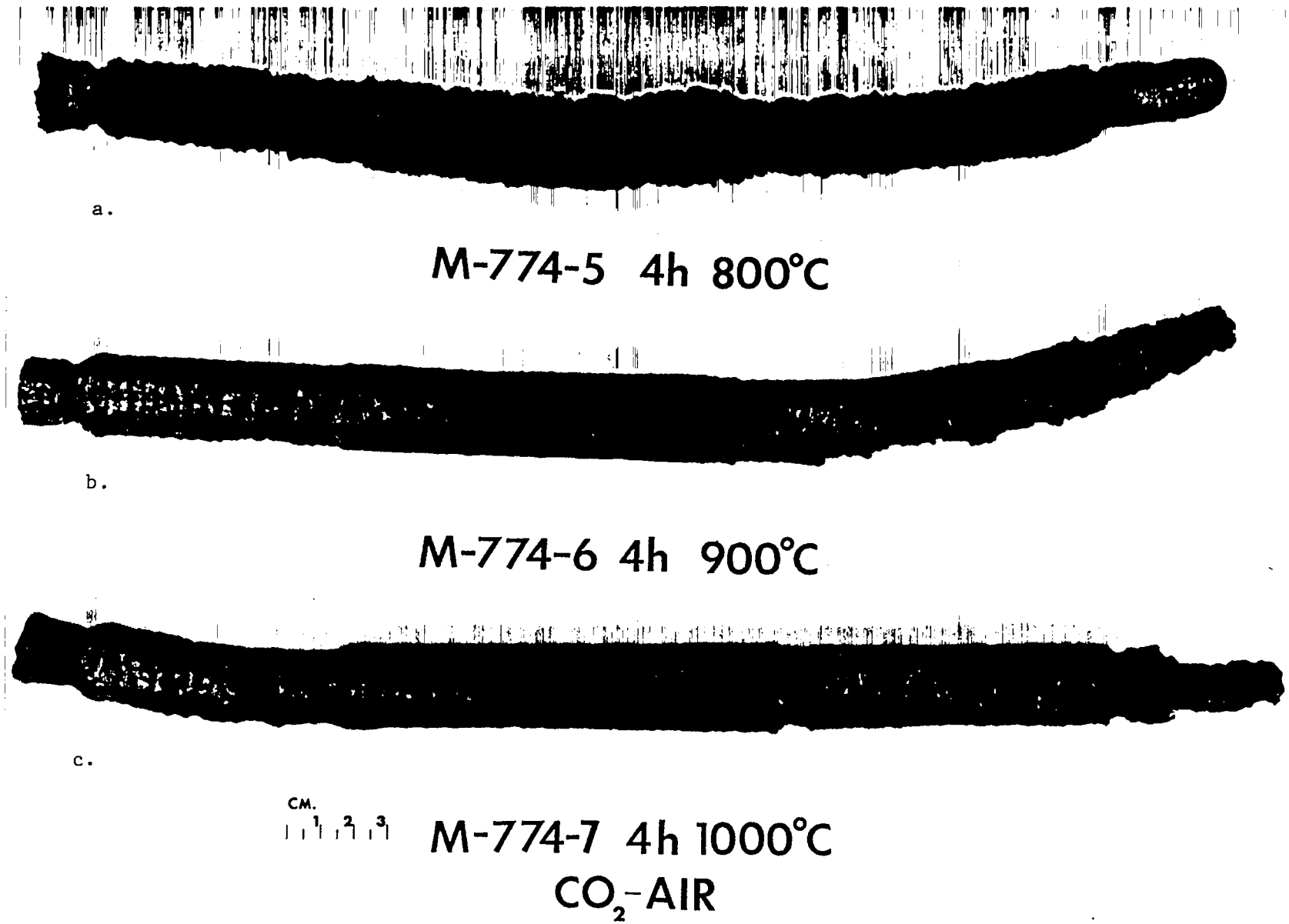

Fig. 15.
Penetrators exposed to CO_2-air mixture at the listed temperature.

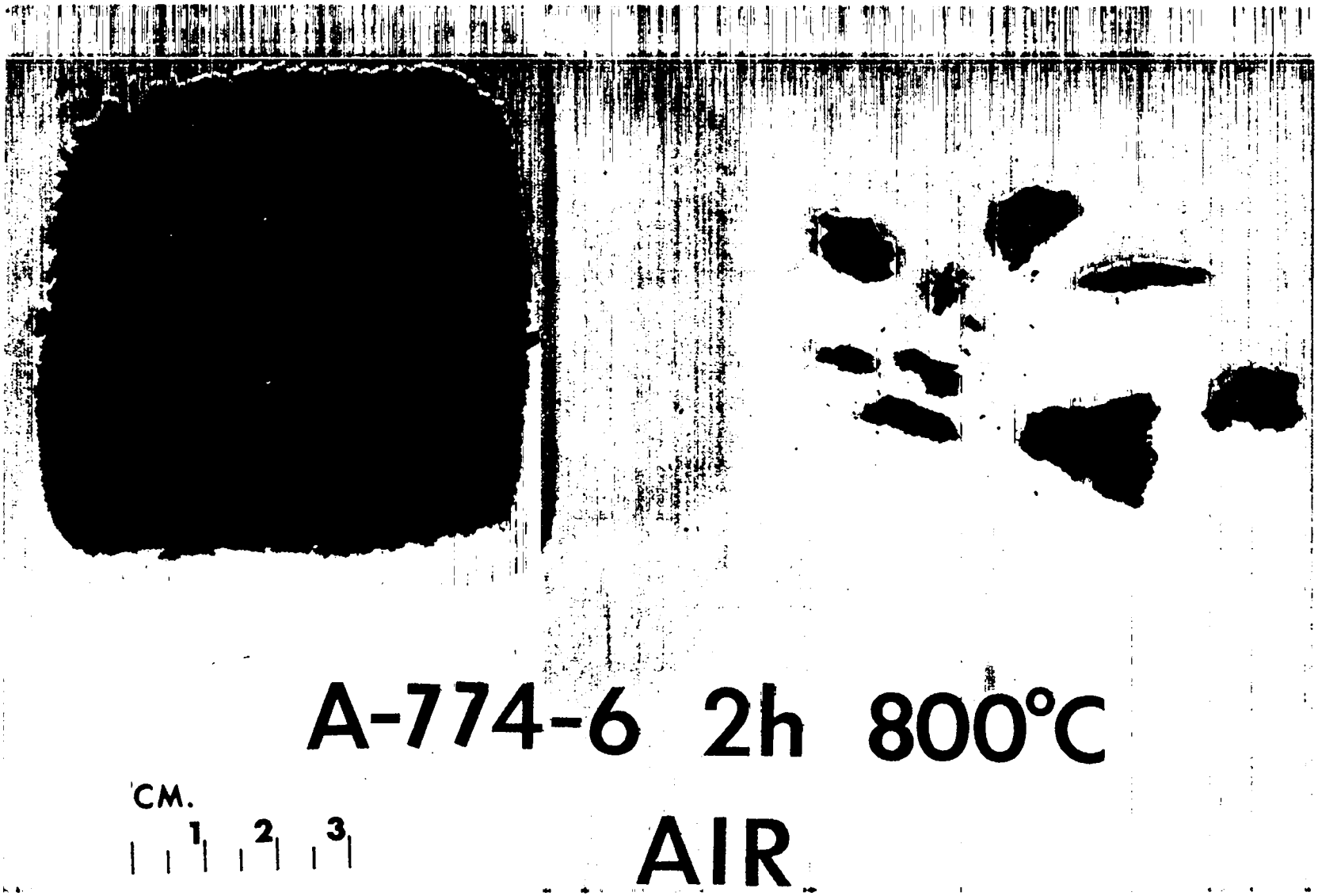

Fig. 16.
Oxide from 800°C air run.

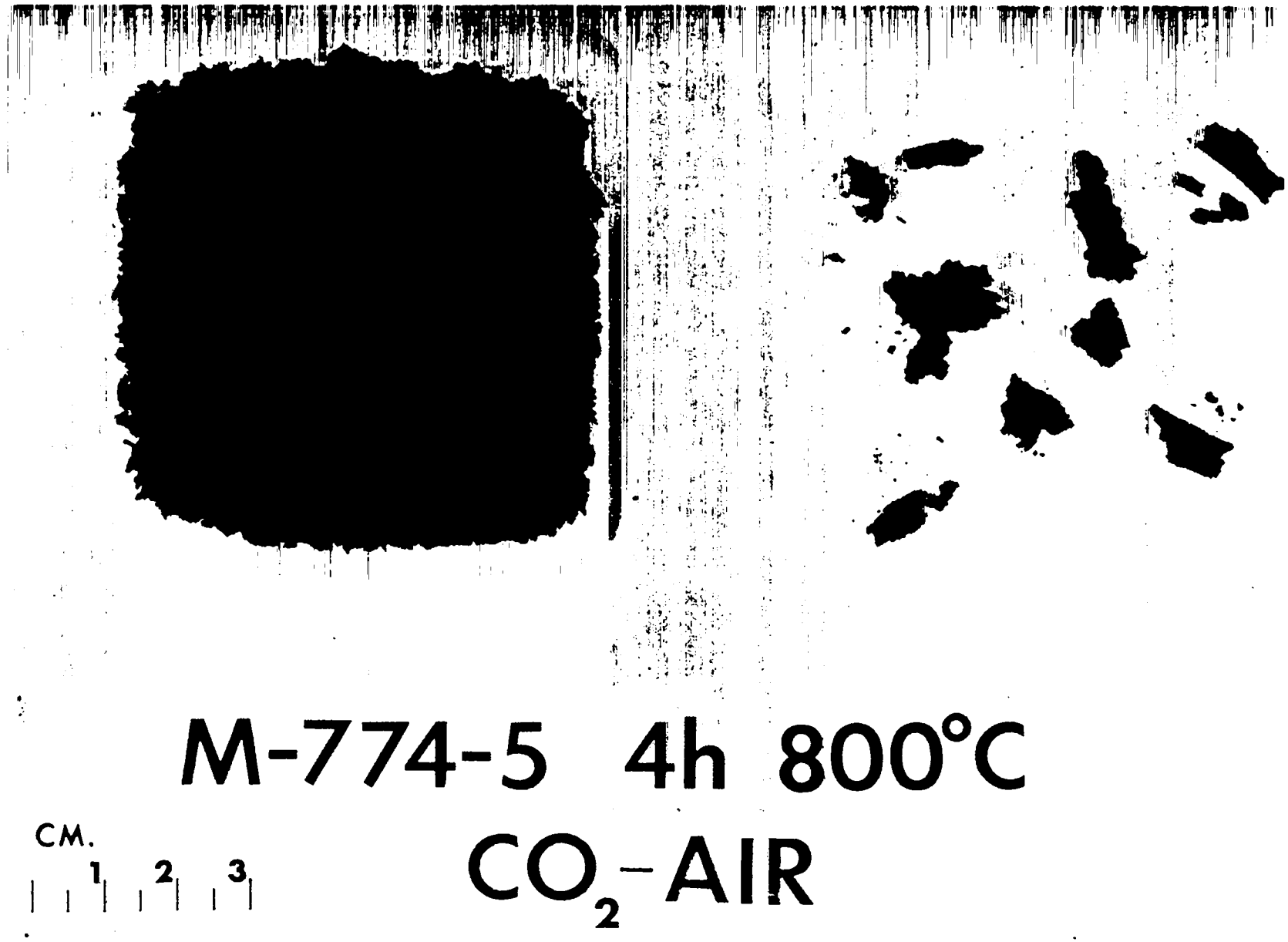

Fig. 17.
Oxide from 800°C CO_2-air run.

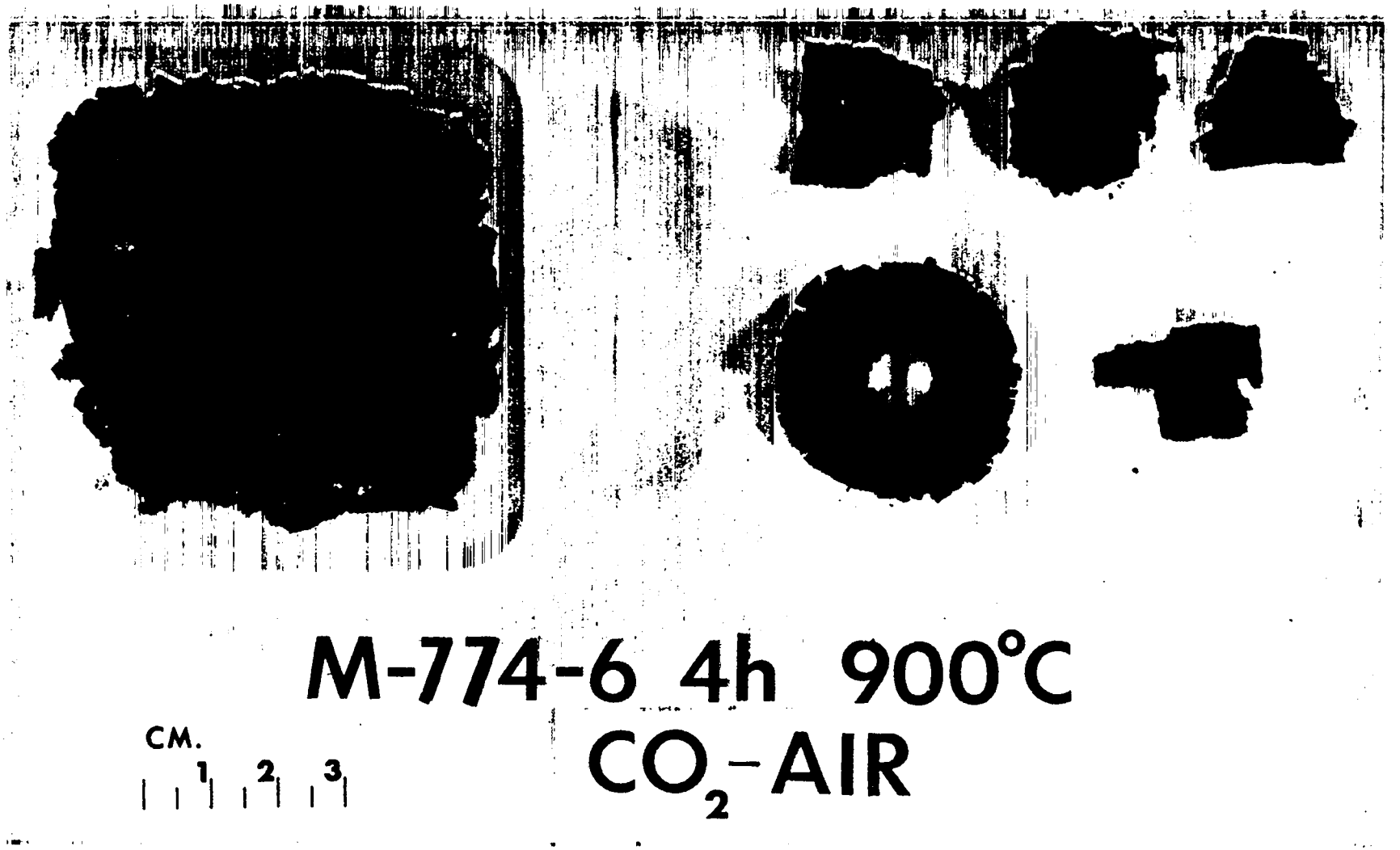

Fig. 18.
Oxide from 900°C CO_2-air run.

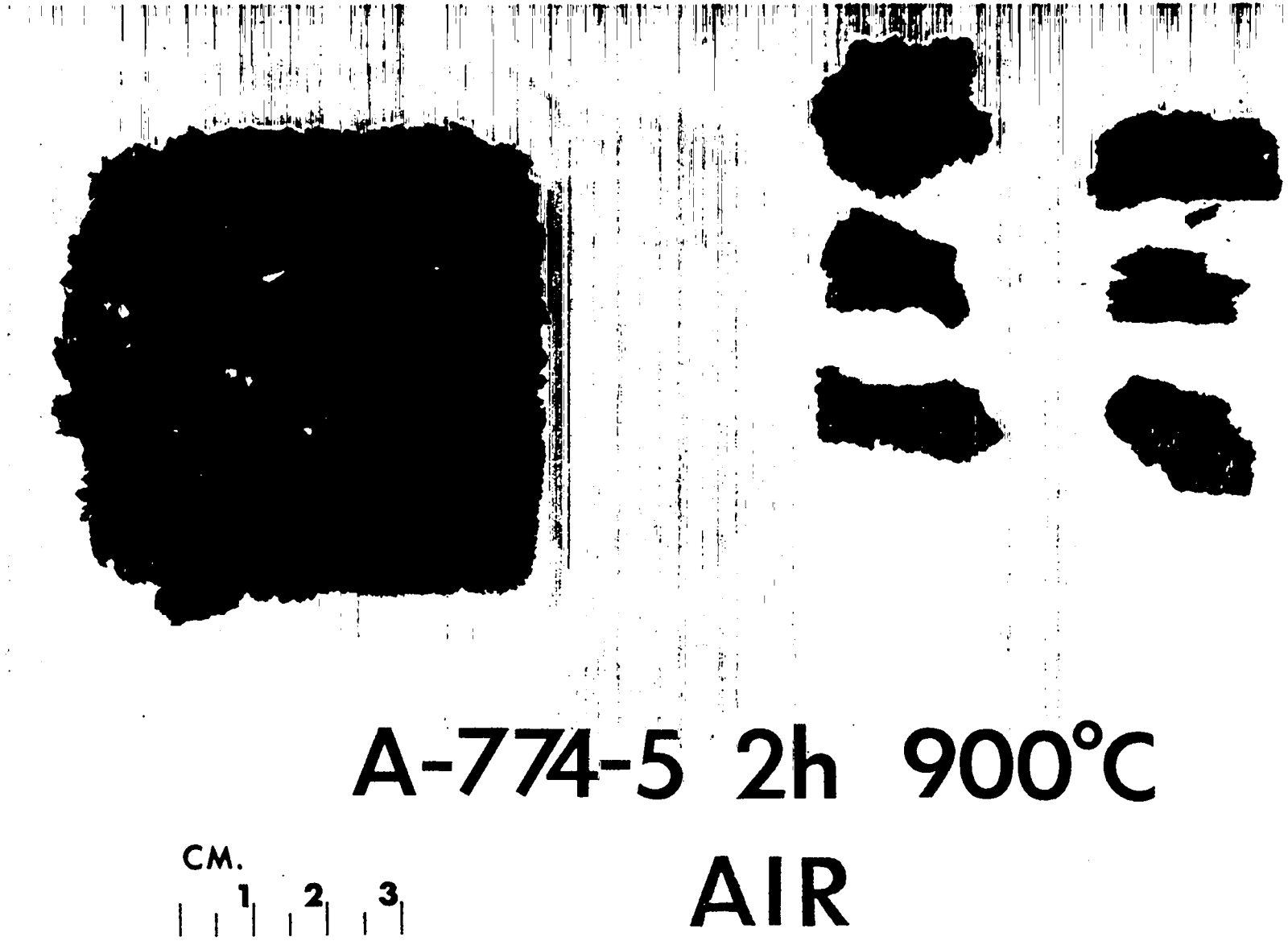

Fig. 19.
Oxide from 900°C air run.

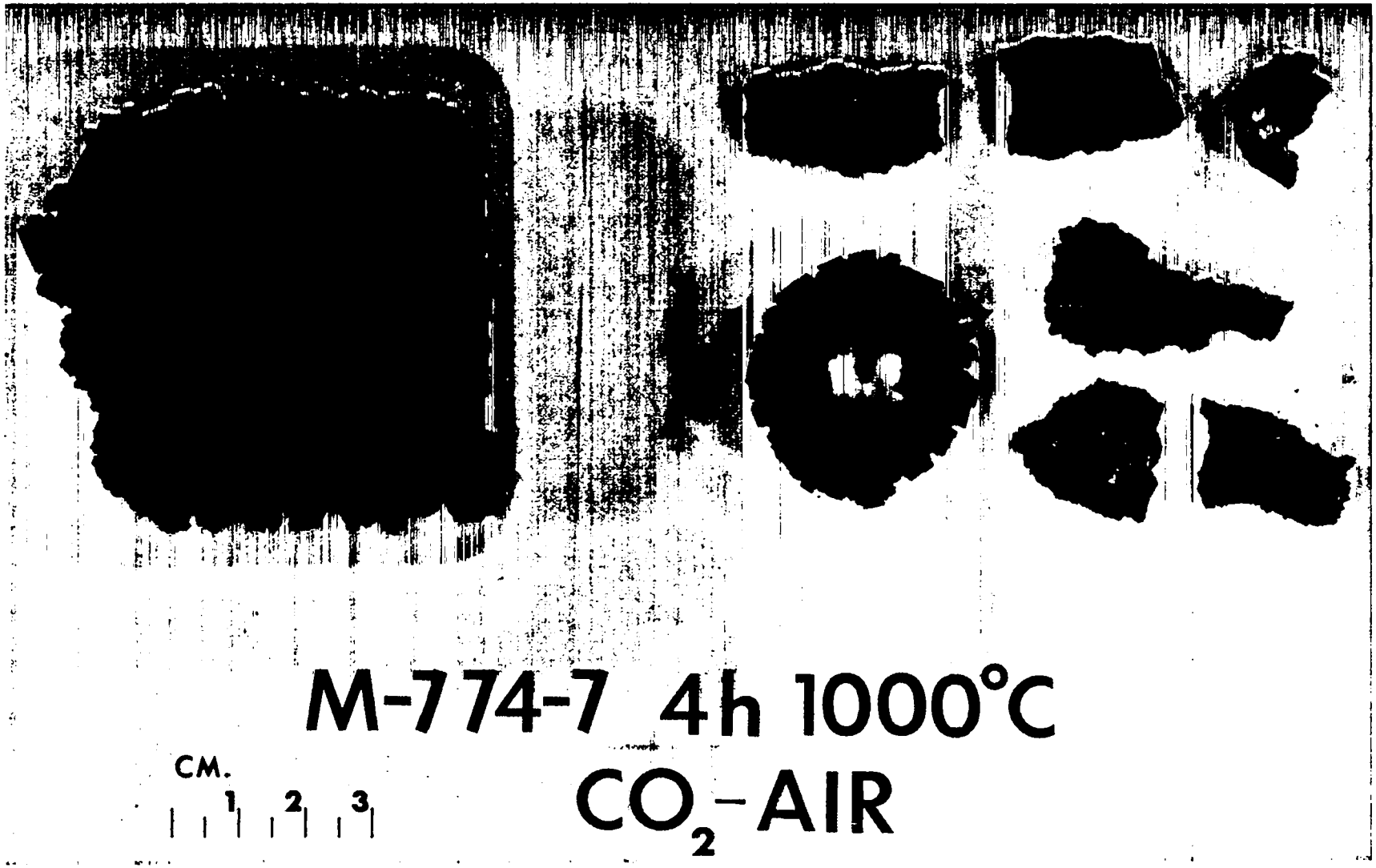

Fig. 20.
Oxide from the 1000°C CO_2-air run.

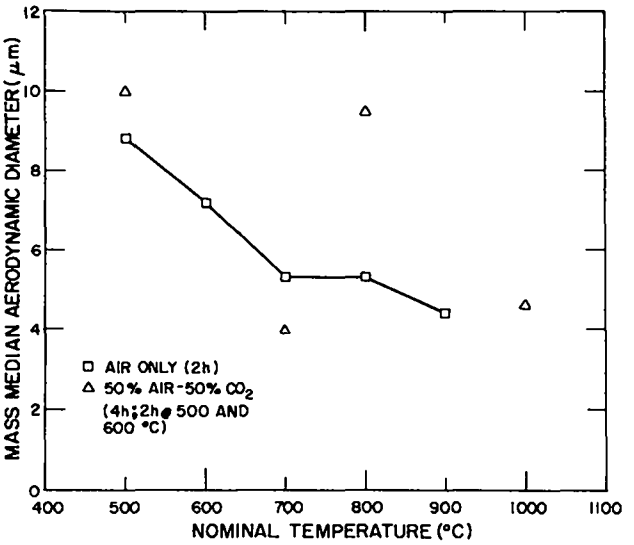

Fig. 21.
Size of aerosol <10-μm as a function of temperature.

somewhat broader size distribution at the 500 to 700°C temperatures than at the 800 to 1000°C temperatures. The mmads for the air runs dropped uniformly from 9 μm to 4.5 μm as temperature was increased from 500 to 900°C. The air-CO_2 results were not consistent with the air-only results at all temperatures, although the mmads remained generally in the same range (4-10 μm). Fewer data made it more difficult to establish a trend for the air-CO_2 results (the 600°C point was omitted because of insufficient mass collected; the 900°C point, because low mass collection in the precutter made the result suspect). Of the four data remaining, only the 800°C result (9.5 μm) differs significantly from the air-only result (5.3 μm). A possible source of variation in the air-CO_2 runs not present in the air runs was a CO_2 bottle change operation, which induced a 75-100°C temperature rise lasting about 1 min. This temperature change may have caused unusual aerosol production because of thermal expansion and contraction at the penetrator surface. Each run had at least one CO_2 bottle change; the 900°C and 1000°C runs each had two changes.

Total aerosol mass collected on all impactor stages, the precutter, and in the high volume sampler is expressed as percent of penetrator mass in Fig. 22. The total mass of aerosol collected ranged between 10^{-4} and 10^{-2}% of penetrator mass, the maximum occurring in the 1000°C air-CO_2 run. The scatter present in the data and different test durations do not permit a clearcut identification of whether there is an effect on aerosol production when CO_2 is added to the atmosphere. The trend of aerosol mass vs temperature was generally the same for the two gas atmospheres if the time differential between 2 and 4 h is taken into account. Aerosol mass was lowest at 500-600°C, increased sharply at 700°C, decreased somewhat at 800°C, and increased again in the 900-1000°C range. The 900°C point from the air-CO_2 runs was not omitted from Fig. 22 as it was from Fig. 21 since the impactor mass had a negligible effect on the results described in Fig. 22.

An estimate of aerosol mass associated with particles smaller than 10 μm as a percent of penetrator mass was obtained by multiplying the fraction of collected aerosol passing the precutter by the total aerosol mass as a percent of penetrator mass (Fig. 23). This result is considered a conservatively high estimate since mass concentration calculated from high volume sampler mass and sample volume exceeded by factors of 3 to 4 the mass concentration calculated similarly from

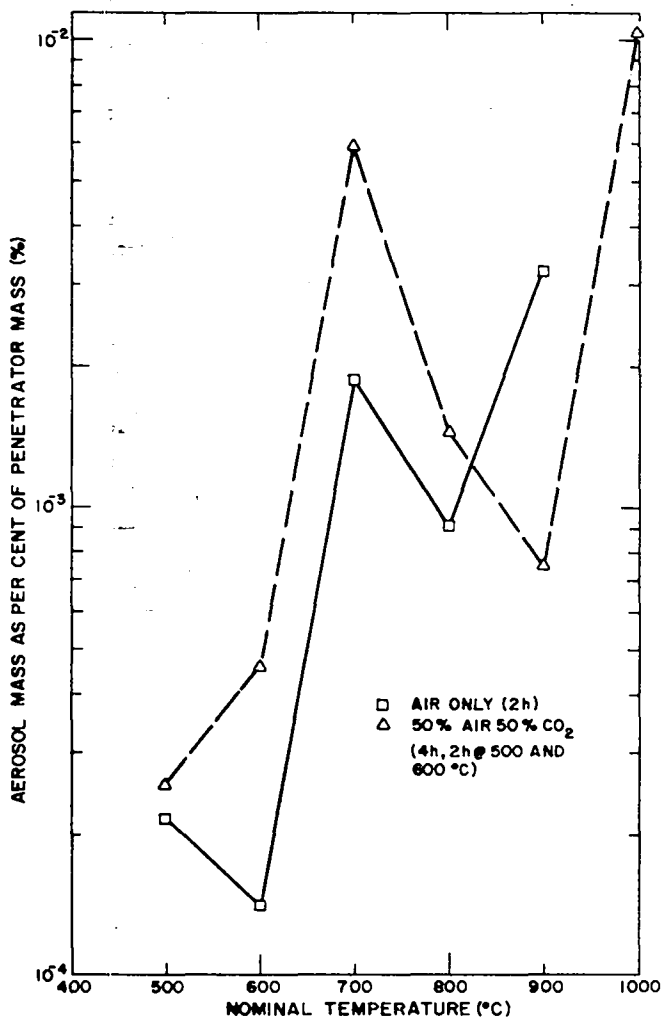

Fig. 22.
Aerosol mass as a function of temperature.

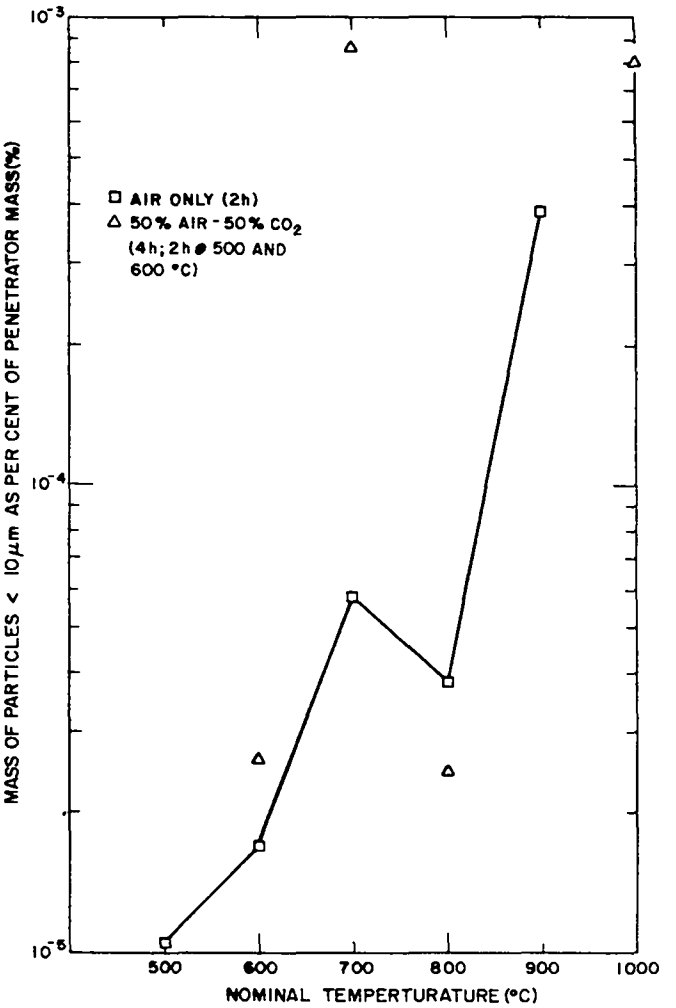

Fig. 23.
Respirable mass as a function of temperature.

impactor data. The probable cause of this discrepancy was placement of the impactor probe at the centerline of the exit tube. Sedimentation of larger particles could be expected to cause higher concentration of larger particles below the centerline of the tube, which the high volume sampler would collect but the impactor would not. The impactor, therefore, provided mass concentration of particles more likely to remain airborne a longer length of time. These estimates in Fig. 23 show a general increase in total mass associated with particles smaller than 10 μm as temperature increases. Again several discrepancies appeared in the data for the reasons described earlier. The very high value for the 700°C air-CO_2 run may be real, in that no experimental problem was identified nor was the mass analysis dubious because of insufficient sample size.

4. Effects of Temperature Change During the Run. Runs at 500 and 700°C in air and 800°C in air-CO_2 were omitted from earlier discussions because each had a temperature irregularity during the run, which prompted repeating the run. Each run showed higher oxidation and aerosol mass than the repeated run at the same nominal temperature. Rapid cooling at some point in the

run apparently caused oxide coating to spall off, exposing new surface to oxidation and aerosolizing more material. The 800°C run showed remarkably high aerosol mass for its short duration (55 min at 800°C plus 18 min cooling to 625°C).

5. Aerosol Production as a Function of Time. Aerosol production as a function of time was first observed on a qualitative basis using the GCA respirable mass monitor. Positive detection of an aerosol occurred within the first 6 min on all runs with nominal temperature of 700°C or above. At lower temperatures, mass concentration was apparently lower than the minimum detection limit of the instrument. The high temperature runs, notably 900 and 1000°C, exhibited positive readings over the first 1 to 2 min after gas flow was initiated, then diminished after 10-15 min. This early production of aerosol prompted another oxidation run at 800°C for 4 h in which high volume samples and aerosol weight percent $<10\ \mu m$ were determined over eight 30-min intervals.

Effects on the penetrator during this run were quite similar to the earlier 800°C run with net metal oxidation of 1011.7 g and 1003.1 g, respectively. Both penetrators were distinctively pitted with large pits. A complete log of data from this run (M-774-8) is included in Table IV.

Aerosol masses collected in the impactor and in the high volume sampler in each of the 30-min intervals are displayed in Fig. 24. The impactor data show a major increase in aerosol mass in the second interval and another increase in the fourth interval. The high volume sampler indicated consistent aerosol mass through the first three intervals followed by a major increase in the fourth interval. The increased amount in the fourth interval coincided with the only CO_2 bottle change and may have been caused by this perturbation. Both samplers indicated a gradual reduction in aerosol production after 2-1/2 h, but did not compare well in the earlier part of the run. Since a vertical mass concentration gradient in the exit tube is probable (as described earlier), the sharp rise in mass collected by the impactor in the second interval may indicate a temporarily higher release of smaller particles. Smaller particles, probably in the range of 10- to 20-μm D_{ae}, could have been collected in higher numbers at the impactor probe inlet without causing a similar large effect in the high volume sampler mass.

The primary results of this experiment are the initiation of aerosol production very early in the exposure period; and the gradual decrease of aerosol production with time after 2-1/2 h.

6. Particle Size Analysis by Sieving. The coarse oxide particles left in the furnace tube or removed from the penetrator by light mechanical work were sieved by standardized methods down to 400 mesh (38 μm). Particle size analysis of sieve weight data was performed as shown in Tyler Screen Scale diagrams attached as Addendum B. Cumulative percent of weight retained was plotted in these diagrams against mesh opening. Midpoint (50%) values from these plots are presented in Fig. 25 to indicate the variation in central tendency of sieve particle size as a function of exposure temperature. Particle size of the sieved oxide from the air-only runs decreased with increasing temperature from 570 μm at 500°C to 180 μm at 700°C. The midpoint size increased at 800 and 900°C. The drop in sieve particle size between the 500 to 600°C runs was more pronounced in the air-CO_2 runs. Results of the no-flow run at 700°C and the air-only run at 700°C were in close agreement, indicating a negligible effect of flow on particle size as defined by sieve analysis.

Megaw[3] observed only an increase in particle size at 600°C and above. Coleman[2] performed similar measurements at 400, 500, and 600°C but did not observe a particle size decrease. The 50% retained sieve size for 600°C in air was compared among these experiments: approximately 130 μm by Coleman, 10-40 μm by Megaw, and 420 μm in this experiment. At 800°C, agreement was no better: 500 μm by Coleman, 80 μm by Megaw, and 240 μm in this experiment. This variation may be caused by differences in sieving practice, that is, percent values in this experiment were based on mass passing a No. 12 screen. The other experimenters may have chosen other methods.

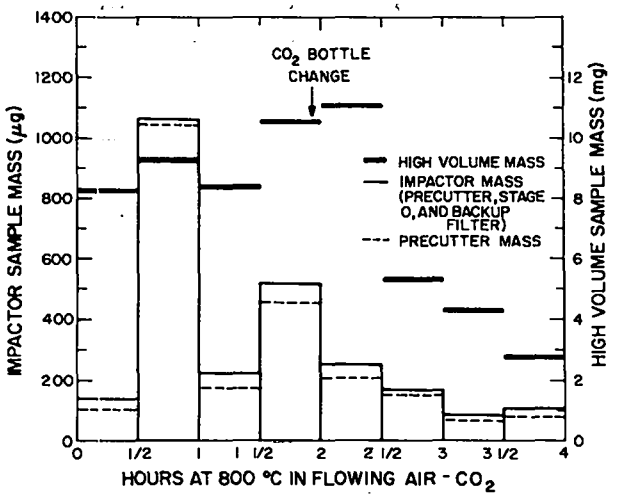

Fig. 24.
Aerosol mass as a function of time.

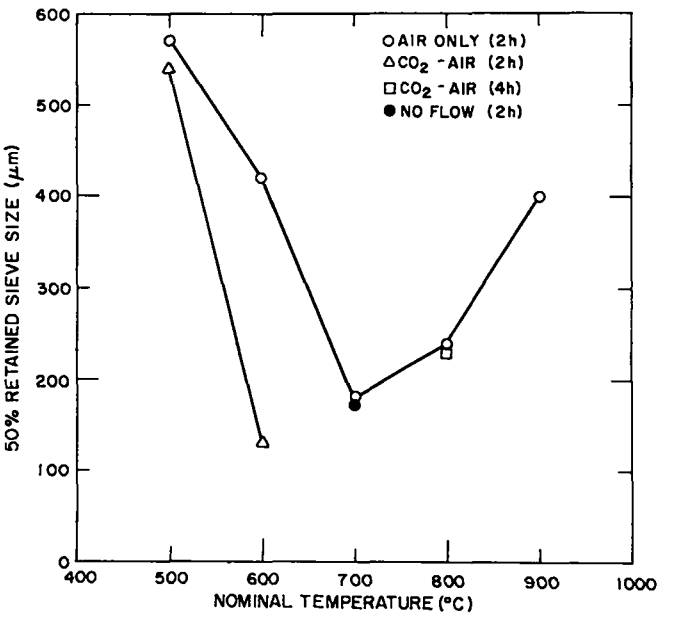

Fig. 25.
Sieve particle size as a function of temperature.

7. **Particle Size Analysis by Sedimentation.** The average Stokes and aerodynamic equivalent diameters of the oxide <38 μm (passing the No. 400 sieve) are displayed as a function of nominal furnace temperature in Fig. 26. Sedimentation analysis permitted assigning an equivalent diameter to each oxide batch in the absence of a detailed particle shape determination.

The D_{ae} increased with increasing temperature from approximately 35 μm at 500°C to 60-65 μm at 800°C. The particle size distribution of the oxide was bimodal. The major and minor mode diameters and the average diameter are included in Fig. 26. The effect of temperature on D_{ae} determined by sedimentation analysis of the mass fraction of oxide <38 μm indicated a different trend than was observed earlier with air samples. The Andersen impactor samples indicated that the mean particle size decreased with increasing temperature while the sedimentation analysis indicates that particle size increased with increasing temperature. However, the sedimentation analysis includes particles that are much larger than the maximum size collected by the impactor, therefore representing a different set of particles. Sedimentation analysis includes particles having D_{ae} over 100 μm while the impactor analysis includes particles having diameters up to 10 μm. The impactor data is more closely related to the minor mode data in which the particle size shows a slight decrease with increasing temperature.

Although there were only two 2-h air-CO_2 runs, the 500°C and 600°C data differed only 10 to 20% from the air-only runs, as shown in Fig. 26. The 4-h air-CO_2 run at 800°C and the no-flow run at 700°C were in close agreement with the air-only runs, showing negligible effect of atmosphere or time-at-temperature in the <400-mesh size range.

Figure 27 shows weight percent for material with <10-μm aerodynamic equivalent diameter estimated from the sedimentation results. This information is of interest as an estimate of the fraction (by weight) of the <38-μm oxide which is in the respirable (<10 μm) range. Also included for comparison is weight fraction of the total oxide which was small enough to pass the 400-mesh sieve. For the air-only runs, the weight percent of the <400-mesh oxide which is in the <10-μm D_{ae} range was 8% at 500°C (0.04% of the total penetrator) and 14% at 900°C (0.07% of the total

penetrator). Comparison of these values to aerosol mass as a percent of penetrator mass in Fig. 23 shows at 900°C only 0.0004% was aerosolized vs 0.07% retained in the oxide; at 500°C, 0.00001% vs 0.04%. Thus, only a small fraction of those DU oxide particles of apparently entrainable size actually became airborne. Other results shown in Fig. 27 were unremarkable except for the large increase of oxide particles <400-mesh produced in the 600°C air-CO_2 (2 h) run. A difference in temperature history during the run is a possible cause; chart records show acceptable control during both runs, except for one extra CO_2 bottle change occurring in the 600°C run.

8. X-Ray Diffraction Analysis of DU Oxide. DU oxide powder samples from the 2-h runs were examined by x-ray diffraction methods principally for phase identification and to ascertain any variations in crystallinity, which might be attributed to temperature history. The principal phase present was U_3O_8 (orthorhombic); however, UO_2 was present in all samples in amounts ranging from a trace to several percent.

All results are summarized in Table V. The effective crystallite size of the U_3O_8 increases with temperature; there appears to be little dependence on the atmosphere or time-at-temperature. The crystallites exhibit much greater perfection in the pole (reference) direction than in any direction perpendicular to this pole, an indication of a columnar, layered configuration. The UO_2 phase increases in relative amount with temperature. The anomolously high relative amount of UO_2 in the 700°C-no airflow sample has no readily apparent cause, but could be due to less available oxygen in the no airflow experiment.

9. Scanning Electron Microscopy (SEM) of DU Oxide. SEM examination of <400-mesh samples was performed for morphological observation only; particle size characterization was not an objective. Oxide particles were manually dispersed from the bulk powder onto an adhesive-coated aluminum specimen stub. While the adhesive was still wet, a mild airstream was blown across the sample by syringe to remove loose material.

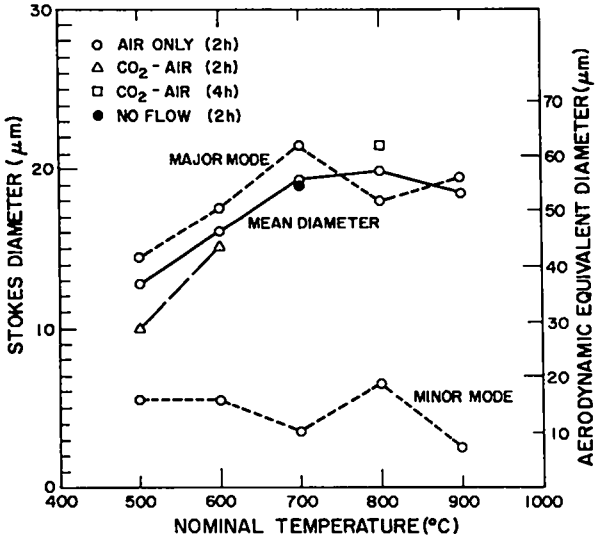

Fig. 26.
Stokes diameter of particles <38 μm as a function of temperature.

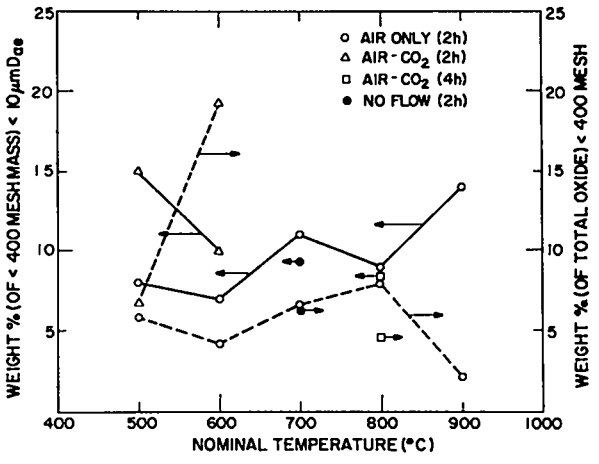

Fig. 27.
Mass distribution in sub-400 mesh sieve fraction.

TABLE V

RESULTS OF X-RAY DIFFRACTION
OF DU OXIDE POWDERS

Sample No.	Test Conditions			Effective Crystallite Size (Å)	Relative UO_2 Amount
	Temp (°C)	Time	Atmosphere		
A-774-7	500	2 h	Air	730	0.35
A-774-2	600	2 h	Air	1100	0.73
A-774-4	700	2 h	Air	1700	0.82
A-774-6	800	2 h	Air	2300	0.99
A-774-5	900	2 h	Air	3800	4.24
M-774-1	500	2 h	50% Air + 50% CO_2	770	0.30
M-774-2	600	2 h	50% Air + 50% CO_2	1350	0.22
M-774-5	800	4 h	50% Air + 50% CO_2	1900	2.54
N-774-1	700	2 h	Air - No Flow	1650	2.19

One photomicrograph from each run has been delivered to ARRADCOM. Particle shape was found to be highly irregular in all runs. Figure 28 shows particles from the penetrator exposure at 500°C in air; Fig. 29, at 700°C in air. The particles formed at 500°C appear smaller, as was expected from the results previously described in Figs. 23 and 26. Particles in the 1- to 10-μm range were usually found, but most particles were in the 10- to 30-μm range. A few needle-like particles as large as 1000 μm in length were present. Submicron particles were rare and usually found on the surface of larger particles. The 500°C specimens appeared to contain higher populations of small particles than the higher temperature runs. Lamellar structure was found in many particles, particularly in the 700, 800, and 900°C photos. Often the lamellae were parallel to the short axis of the particle. A variety of particle shapes appeared to be present (leaf-like, needle, and equiaxial); these could not be characterized in detail by this SEM examination.

IV. SUMMARY AND CONCLUSIONS

These forced-draft oxidation experiments indicated DU aerosols were dispersed at all temperatures in the range 500 to 1000°C. An outdoor burning experiment (Burn 4) with peak temperatures near 1100°C and broad temperature cycles oxidized 42-47% of original penetrator weight in 3 h, compared to a maximum of 30% in 4 h in the 800°C laboratory experiment where a uniform temperature was controlled. Burn 4 also produced more aerosol mass in the respirable size range (up to 62% of the total aerosol mass was associated with particles under 10-μm D_{ae}, compared to a maximum of 14% in the laboratory experiments).

Gravimetric analysis of DU metal removed as oxide in the 2-h air-only experiments showed oxidation increased by a factor of approximately three between 600 and 700°C to a maximum of 22% at 700°C. The 4-h air-CO_2 experiments showed a similar increase started between 600 and 700°C and reached a maximum of 30% at 800°C. Decreasing oxidation at higher temperatures probably indicated a change in the oxide layer, which tended to protect the penetrator. This general trend of maximum oxidation at 700 or 800°C agreed with Megaw results[8] although these results did not have sufficient detail to show that the maximum occurred at the beta-gamma transition temperature of 771°C, as Megaw suggested.

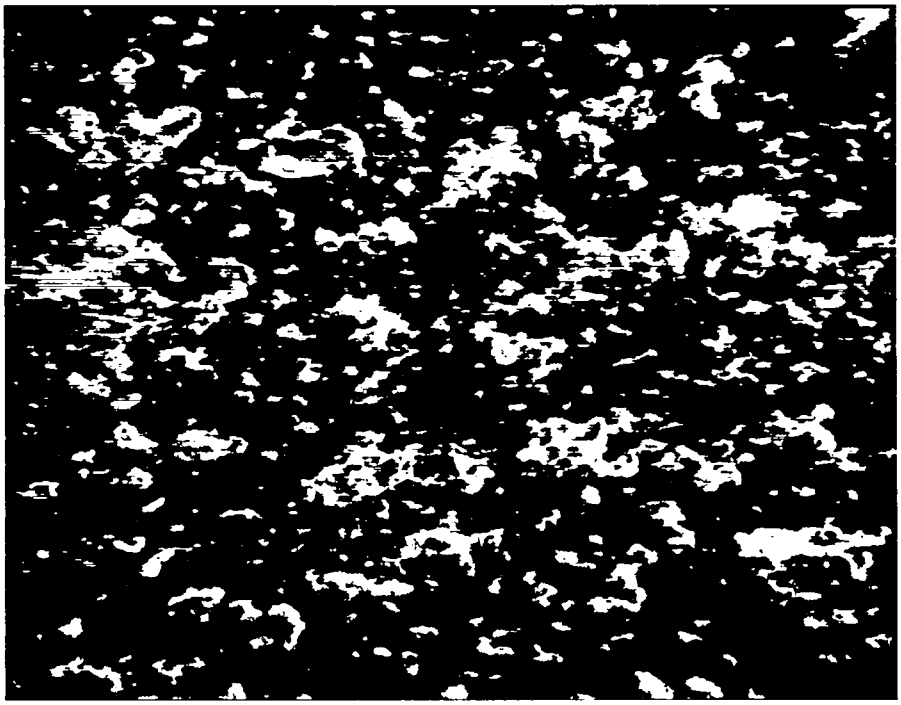

Fig. 28.
Particles from 500°C exposure in air.

Fig. 29.
Particles from 700°C exposure in air.

Mass median aerodynamic diameter of the DU aerosol passing the 10-μm precutter of the impactor decreased with increasing temperature from 10 μm to 4 μm. Geometric standard deviation of these aerosols ranged from 1.7 to 3.6. Mass of aerosol particles <10-μm D_{ae} as percent of penetrator mass ranged from approximately 10^{-5}% at 500°C to 10^{-3}% at 1000°C. The effect on aerosol size characteristics of CO_2 in the atmosphere was difficult to determine because of the run time change from 2 to 4 h after the air-only runs were completed.

Nonairborne oxide particles exhibited a decrease in median size (50% retained sieve size) between 500 and 600°C followed by an increase in size at higher temperatures. This median particle size range was approximately 100-600 μm. The referenced studies[2,3] both found that particle size increased with increasing temperature.

The particle fraction passing the finest sieve (<38-μm linear dimension) was subjected to size analysis by sedimentation techniques. This analysis indicated that D_{ae} increased from approximately 35 μm at 500°C to 60-65 μm at 800°C. The particle size distribution was bimodal in this size range with the minor mode generally 10- to 20-μm D_{ae}. The presence of major amounts of particles <10-μm D_{ae} in this fraction indicates only a small fraction of oxide particles of apparently entrainable size actually became airborne.

General conclusions to be drawn from these experiments with bare penetrators are as follows:

(1) DU aerosols with particles in the respirable size range are produced when penetrators are exposed to temperatures above 500°C for times on the order of one-half hour or more.

(2) Production of the oxide and of aerosol was enhanced by forced-draft and temperature cycling during exposure of penetrators under fire conditions.

(3) Penetrators did not exhibit any tendency toward self-sustained burning, although complete oxidation could no doubt be achieved if adequate fuel and time (longer than 4 h) were provided.

ACKNOWLEDGMENTS

Our sincere thanks go to the following people who contributed significantly to this project: Ernest Bloore and Ed Wilsey, ARRADCOM; Joe Greene, M-2; Dick Heaton, Hal Ide, Jean Lindsey, H-5; John Magnuson, CMB-6; Leonard Levinson and John O'Rourke, CMB-8.

REFERENCES

1. J. Katz and E. Rabinowitz, **The Chemistry of Uranium**, p. 165, McGraw-Hill, New York, 1951.

2. L. F. Coleman and L. C. Schwendiman, "Particles Generated During the Air Oxidation of Uranium," Hanford Laboratories report HW-SA-2641, August 1962.

3. W. J. Megaw, R. C. Chadwick, A. C. Wells, and J. E. Bridges, "The Oxidation and Release of Iodine-131 From Uranium Slugs Oxidizing in Air and Carbon Dioxide," Reactor Science and Technology (Journal of Nuclear Energy Parts A/B) **15**, 176-184 (1961).

4. H. M. Ide, W. D. Moss, M. M. Minor, and E. E. Campbell, "Analysis of Uranium in Urine by Delayed Neutrons," Health Phys. **37**, 405-408 (1979).

5. ASTM Specification E-11-70, "USA Sieve Series."

6. Commercial Bulletin, "Sedimentation Balance for Automatic Determination of Particle Size Distribution," Sartorius-Werke AG, Gottingen, West Germany.

ADDENDUM A

Temperature Chart Records

Burn 4

TEMPERATURE HISTORY OF

MIDDLE PENETRATOR

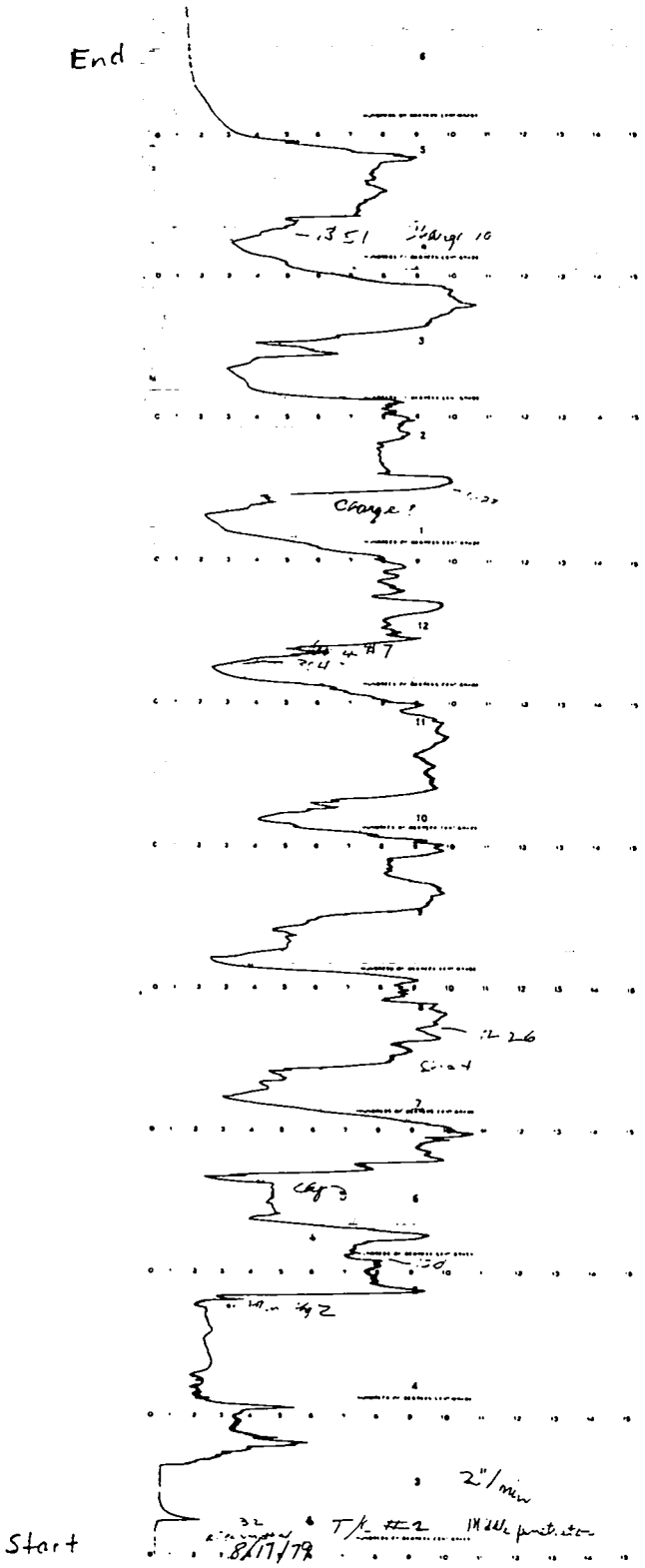

TEMPERATURE HISTORY OF

TOP PENETRATOR

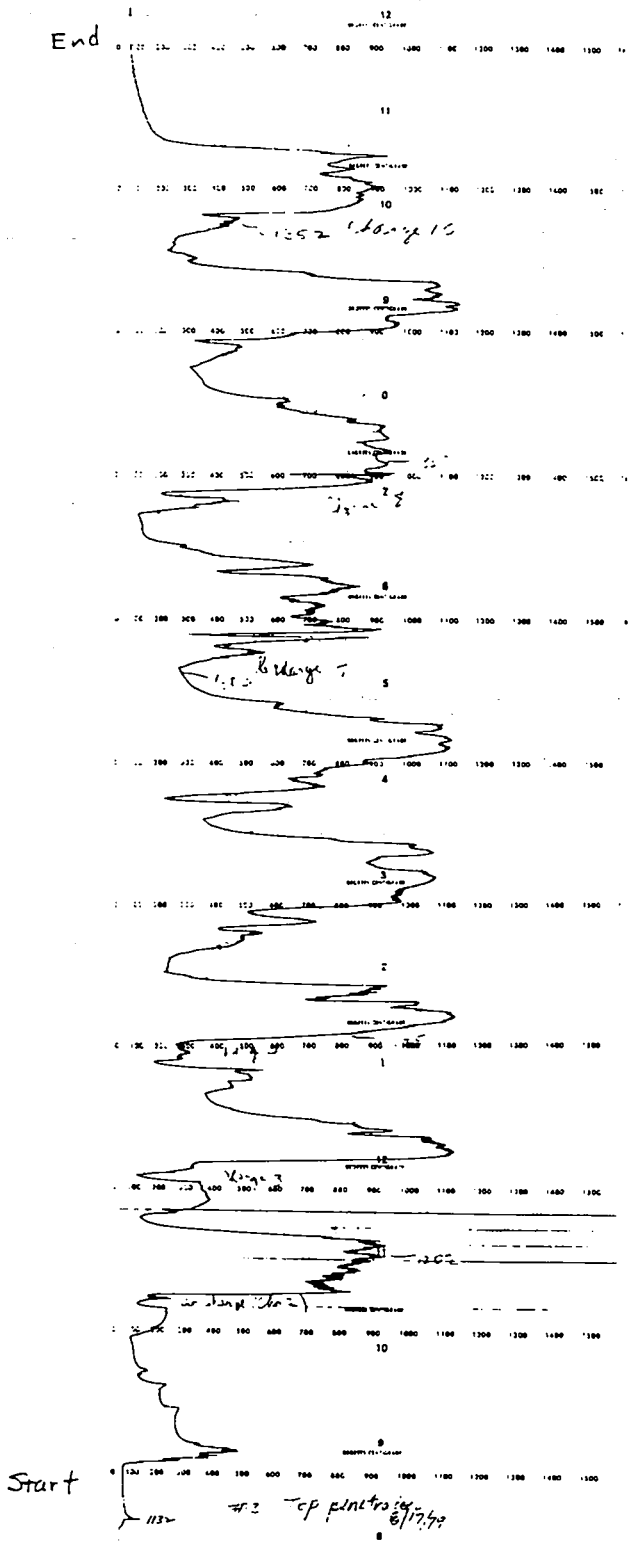

ADDENDUM B

Sieving Diagrams for Air-Only, CO_2-Air at 800°C, and No Flow Runs

The Tyler Standard Screen Scale

Form No. L-6
Please mention above when ordering

Cumulative Logarithmic Diagram of Screen Analysis on Sample of depleted U_3O_8 L-6

Name Air Only Date 8/1/79

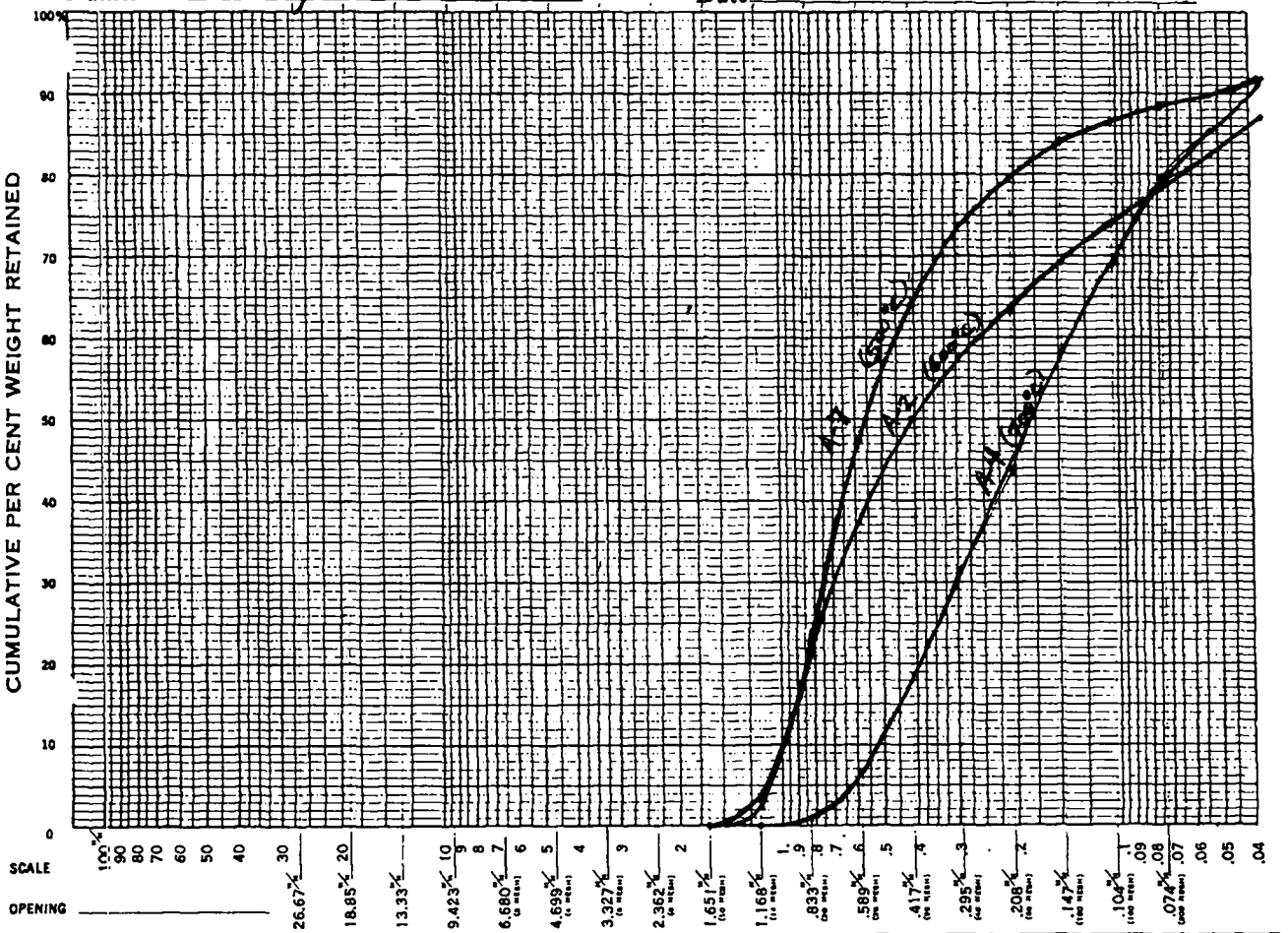

	SCREEN SCALE RATIO 1.414				A-774-7 (500°C)			A-774-2 (600°C)			A-774-4 (700°C)		
	Openings Milli-meters	Openings Inches	Tyler Mesh	U. S. No.	Sample Weights	Per Cent	Per Cent Cumulative Weights	Sample Weights	Per Cent	Per Cent Cumulative Weights	Sample Weights	Per Cent	Per Cent Cumulative Weights
	26.67	1.050	Fragments			61.4 g			157.1 g			97.0 g	
	18.85	.742	> #	12									
	13.33	.525	Total	oxide		266.9 g			236.3 g			854.1 g	
	9.423	.371											
	6.680	.263	3										
	4.699	.185	4	4									
	3.327	.131	6	6									
	2.362	.093	8	8									
ON	1.651	.065	10	12	0.0	0.0	0.0	0.0	0.0	0.0	0.0	0.0	0.0
"	1.168	.046	14	16	2.3	2.3	2.3	2.7	3.5	3.5	0.0	0.0	0.0
"	.833	.0328	20	20	20.5	20.6	22.9	13.6	17.5	21.0	0.8	0.8	0.8
"	.589	.0232	28	30	24.2	24.3	47.2	12.7	16.4	37.4	5.9	5.9	6.7
"	.417	.0164	35	40	16.7	16.8	64.0	9.8	12.6	50.0	11.9	12.0	18.7
"	.295	.0116	48	50	9.5	9.6	73.6	6.0	7.7	57.7	12.8	12.9	31.6
"	.208	.0082	65	70	6.2	6.2	79.8	4.2	5.4	63.1	11.8	11.9	43.4
"	.147	.0058	100	100	4.5	4.5	84.3	4.7	6.1	69.2	15.0	15.1	58.5
"	.104	.0041	150	140	2.2	2.2	86.5	3.8	4.9	74.1	10.5	10.5	69.0
"	.074	.0029	200	200	2.1	2.1	88.6	3.8	4.9	79.0	10.7	10.7	79.7
"	.053		270	270	1.2	1.2	89.8	2.6	3.4	82.4	6.9	5.9	85.6
"	.038		400	400	2.2	2.2	92.0	3.8	4.9	87.3	6.2	6.2	91.8
Pass	.038		400	400	7.9	7.9	99.9	9.8	12.6	99.9	8.1	8.1	99.9

The Tyler Standard Screen Scale

Form No. L-6
Please mention above when ordering

Cumulative Logarithmic Diagram of Screen Analysis on Sample of Depleted U_3O_8 L-6

Name 50% Air – 50% CO_2 Date 8/1/79

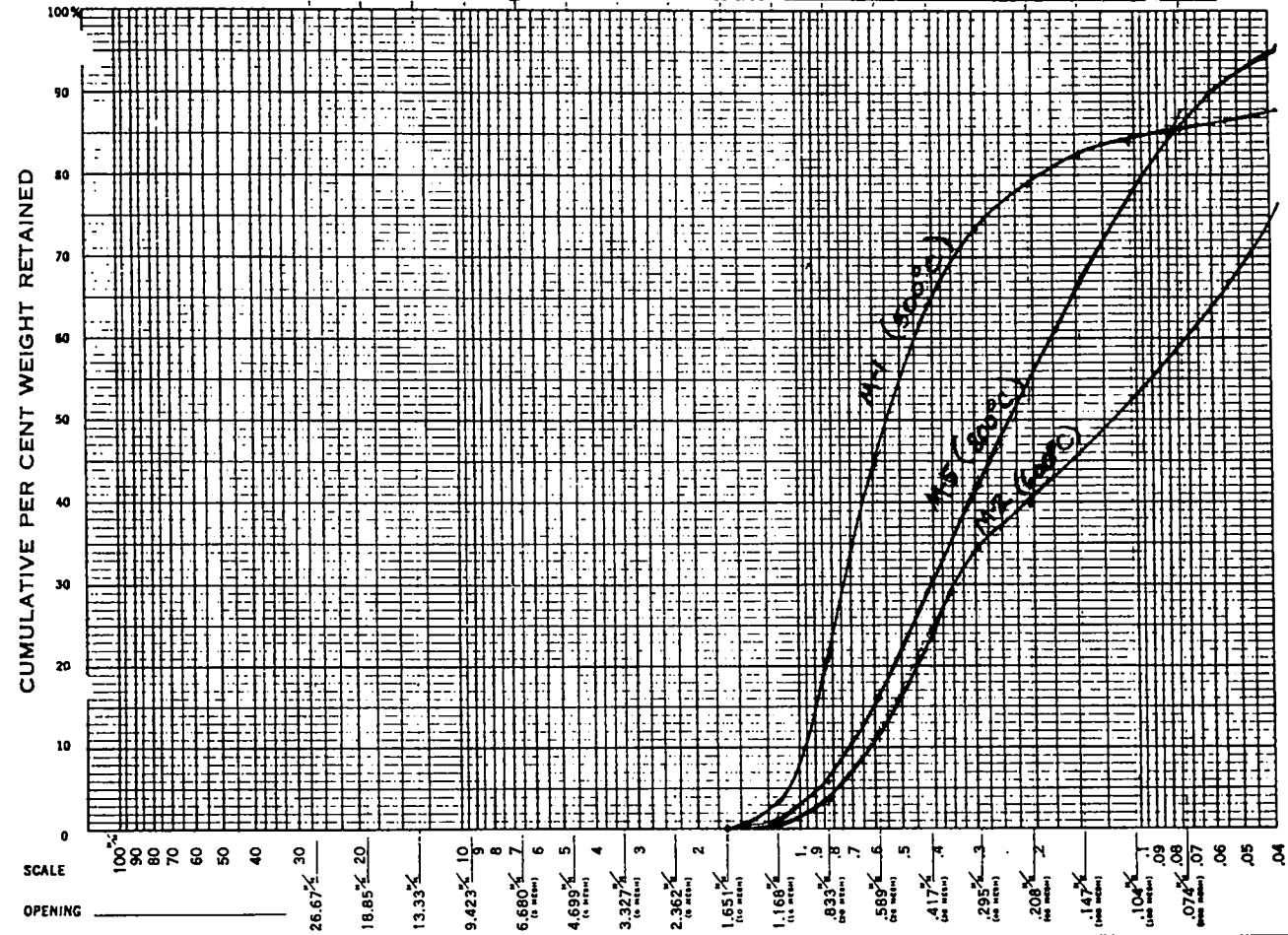

	SCREEN SCALE RATIO 1.414				M-774-1 (500°C) 2h			M-774-2 (600°C) 2h			M-774-5 (800°C) 4h		
	Openings		Tyler Mesh	U. S. No.	Sample Weights	Per Cent	Per Cent Cumulative Weights	Sample Weights	Per Cent	Per Cent Cumulative Weights	Sample Weights	Per Cent	Per Cent Cumulative Weights
	Milli-meters	Inches											
	26.67	1.050	Fragments			94.6g			46.8g			183.8g	
	18.85	.742	> # 12										
	13.33	.525	Total	oxide		235.1g			242.1g			1132.8g	
	9.423	.371											
	6.680	.263	3										
	4.699	.185	4	4									
	3.327	.131	6	6									
	2.362	.093	8	8									
ON	1.651	.065	10	12	0.0	0.0	0.0	0.0	0.0	0.0	0.0	0.0	0.0
"	1.168	.046	14	16	3.3	3.3	3.3	0.3	0.3	0.3	1.0	1.0	1.0
"	.833	.0328	20	20	19.6	17.6	20.9	3.0	3.0	3.3	5.8	5.8	6.8
"	.589	.0232	28	30	24.9	24.9	45.8	8.3	8.3	11.6	9.2	9.2	16.0
"	.417	.0164	35	40	18.2	18.2	64.0	12.8	12.8	24.4	14.4	14.4	30.4
"	.295	.0116	48	50	9.4	9.4	73.4	9.7	9.7	34.1	12.0	12.0	42.0
"	.208	.0082	65	70	5.4	5.4	78.8	5.8	5.8	39.9	9.9	9.9	52.2
"	.147	.0058	100	100	3.4	3.4	82.2	7.0	7.0	46.9	14.3	14.3	66.6
"	.104	.0041	150	140	1.8	1.8	84.0	6.0	6.0	52.9	11.3	11.3	77.9
"	.074	.0029	200	200	1.5	1.5	85.5	7.8	7.8	60.7	9.6	9.6	87.5
Loss #	.053		270	270	10.9	0.9	96.4	6.0	6.0	66.7	4.2	4.2	91.7
"	.038		400	400	1.5	1.5	97.9	9.7	9.7	76.4	3.7	3.7	95.4
Pass	.038		400	400	12.1	12.1	100	23.6	23.6	100	4.5	4.5	99.9

The Tyler Standard Screen Scale

Form No. L-4
Please mention above when ordering

L-6

Cumulative Logarithmic Diagram of Screen Analysis on Sample of Depleted U_3O_8

Name A-774- Air Only No flow Date 8/1/79

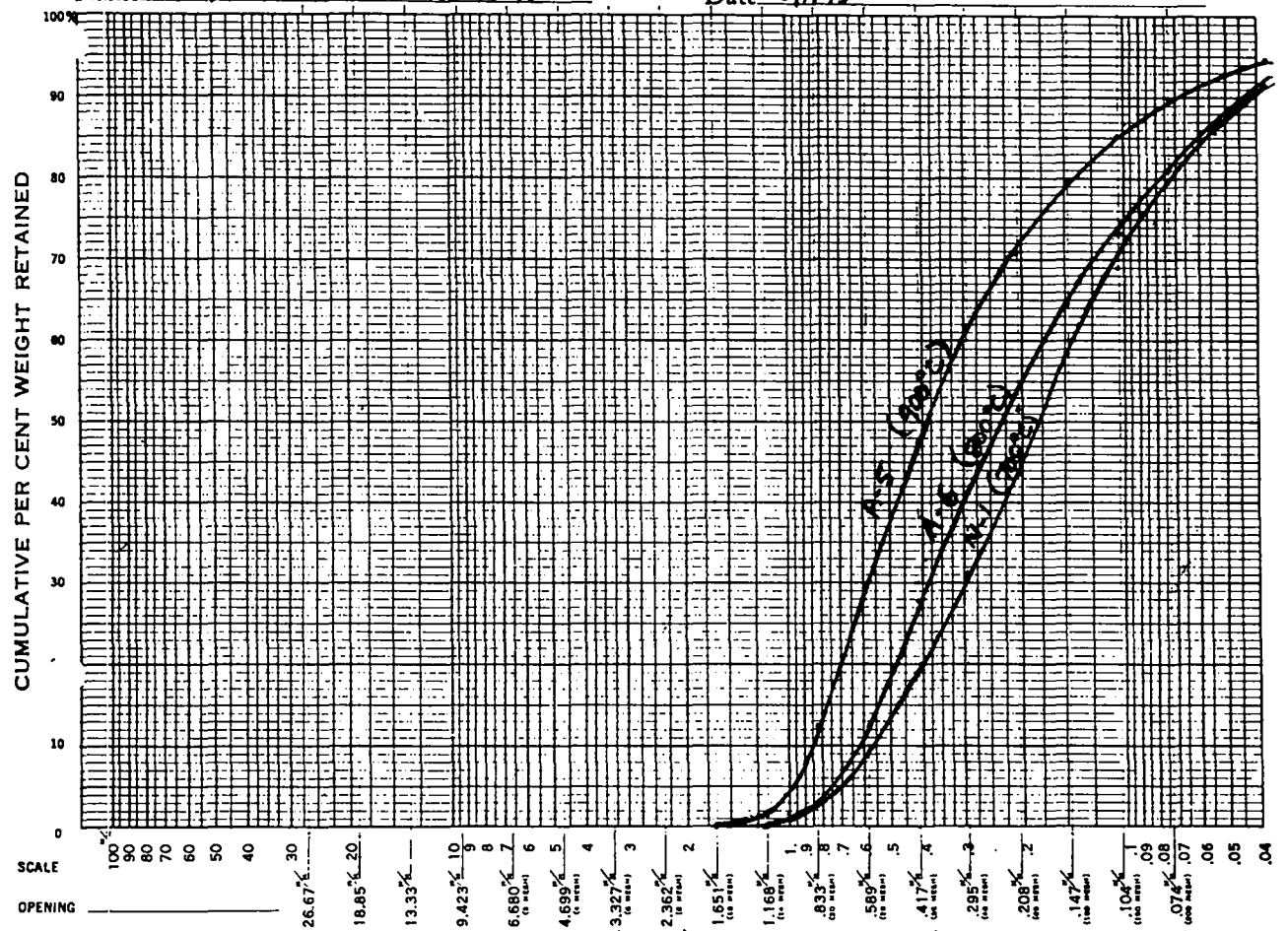

	SCREEN SCALE RATIO 1.414				A-774-6 (800°C)			A-774-5 (900°C)			N-774-1 (700°C) No flow		
	Openings		Tyler Mesh	U.S. No.	Sample Weights	Per Cent	Per Cent Cumulative Weights	Sample Weights	Per Cent	Per Cent Cumulative Weights	Sample Weights	Per Cent	Per Cent Cumulative Weights
	Milli-meters	Inches											
	26.67	1.050	Fragments			87.6g			272.3g			90.3g	
	18.85	.742	7# 12										
	13.33	.525	Total oxide			670.1g			575.3g			495.0g	
	9.423	.371											
	6.680	.263	3										
	4.699	.185	4	4									
	3.327	.131	6	6									
	2.362	.093	8	8									
ON	1.651	.065	10	12	0.0	0.0	0.0	0.0	0.0	0.0	0.0	0.0	0.0
"	1.168	.046	14	16	0.2	0.2	0.2	1.3	1.3	1.3	0.1	0.1	0.1
"	.833	.0328	20	20	2.1	2.1	2.3	11.3	11.3	12.6	2.3	2.3	2.4
"	.589	.0232	28	30	6.3	6.3	8.6	16.7	16.7	29.3	9.7	9.7	12.1
"	.417	.0164	35	40	10.7	10.7	19.3	17.8	17.8	47.1	15.8	15.8	27.9
"	.295	.0116	48	50	11.9	11.9	31.2	14.0	14.0	61.1	13.2	13.2	41.1
"	.208	.0082	65	70	12.1	12.1	43.3	9.6	9.6	70.7	10.5	10.5	51.6
"	.147	.0058	100	100	15.1	15.1	58.4	9.2	9.2	79.9	12.6	12.6	64.2
"	.104	.0041	150	140	10.6	10.6	69.0	5.2	5.2	85.1	9.0	9.0	73.2
"	.074	.0029	200	200	10.6	10.6	79.6	4.6	4.6	89.7	8.4	8.4	81.6
"	.053		270	270	5.7	5.7	85.3	2.4	2.4	92.1	4.6	4.6	86.2
"	.038		400	400	5.8	5.8	91.1	2.6	2.6	94.7	5.2	5.2	91.4
Pass	.038		400	400	8.9	8.9	100.0	5.2	5.2	99.9	8.5	8.5	99.9

U.S. ARMY DISTRIBUTION LIST

Office of Secretary of Defense
(Health Affairs)
ATTN: LTC B. Chase
Pentagon, Room E171
Washington, DC 20301

Office of Secretary of Defense
Office of Director of Defense
Research and Engineering
ATTN: Mr. J. Persh
Engineering
Washington, DC 20301

Office of Assistant Secretary
of Defense for Atomic Energy
ATTN: Cmdr. G. Cliff
Pentagon, Room 3E1069
Washington, DC 20301

Honorable Percy A. Pierre
Assistant Secretary of the Army
for Research, Development
and Acquisition
Department of the Army
Washington, DC 20301

Office of the Undersecretary
of the Army
Deputy Undersecretary (Operations)
Research
ATTN: Mr. D. Hardison
Department of the Army
Washington, DC 20310

Undersecretary of Defense for
Research and Engineering
Deputy Undersecretary
(Tactical Warfare Programs)
Department of Defense
Washington, DC 20310

Director
Defense Advanced Research Projects
Agency
ATTN: Tech Info
1400 Wilson Blvd.
Arlington, VA 22209

Undersecretary of Defense for
Research and Engineering
Deputy Undersecretary (Research
and Advanced Technology)
ATTN: Dr. A. Bement
Department of Defense
Washington, DC 20301

Office of the Deputy Undersecretary
of Defense, Research and

ATTN: Mr. R. Thorkildsen
Pentagon
Washington, DC 20301

Headquarters
Department of the Army
ATTN: DASG-TSP-E, COL Wangeman
Washington, DC 20310

Headquarters
Department of the Army
ATTN: DACS-DMT
Washington, DC 20310

Headquarters
Department of the Army
ATTN: DAMA-ARX-A, Dr. M. Lasser
Washington, DC 20310

Headquarters
Department of the Army
ATTN: DAMA-CSS, Dr. J. Bryant
Washington, DC 20310

Headquarters
Department of the Army
ATTN: DAMA-CSM, LTC German
Washington, DC 20310

Headquarters
Department of the Army
ATTN: DAMA-CSM-CA, Mr. Lippi
Washington, DC 20310

Headquarters
Department of the Army
ATTN: DAMA-WSW, LTC Hinson
Washington, DC 20310

Headquarters
Department of the Army
ATTN: DAMA-WSZ-A
Washington, DC 20310

Headquarters
Department of the Army
ATTN: DAMO-RQD, LTC Ivey
Washington, DC 20310

Headquarters
Department of the Army
ATTN: DAMO-TRS, LTC Lyon
Washington, DC 20310

Headquarters
Department of the Army
ATTN: DAMO-DRI, MAJ Speedy
Washington, DC 20310

Headquarters
Department of the Army
ATTN: DALO-TSP, LTC Eakery
Washington, DC 20310

Headquarters
Department of the Army
ATTN: DALO-SMS, Ms. Ueckert
Washington, DC 20310

Headquarters
Department of the Army
ATTN: DACS-DPA, LTC Rogers
Washington, DC 20310

Headquarters
Department of the Army
ATTN: DAEN-ZE, COL Herndon
Washington, DC 20310

Headquarters
Department of the Army
ATTN: SARDA, COL D. Brudvig
Washington, DC 20310

Project Manager
XM1 Tank Armament System
ATTN: DRCPM-GCM
WArren, MI 48092

Project Manager
XM1 Tank System
ATTN: DRCPM-GCM-SI
Mr. D. Bartle
Warren, MI 48090

Project Manager
Tank Main Armament System
ATTN: DRCPM-TMA, COL D. Appling
Dover, NJ 07801

Project Manager
Tank Main Armament System
ATTN: DRCPM-TMA 105mm
LTC M. Michlik
Dover, NJ 07801

Project Manager
Division Air Defense Gun
ATTN: DRCPM-ADG
Dover, NJ 07801

Project Manager
Production Base Modernization and Exp
ATTN: SARPM-PBM, Mr. C. Kolis
Dover, NJ 07801

Project Manager
M60 Tank
Michigan Army Missile Plant
ATTN: DRCPM-M60
Warren, MI 48090

Commander
US Army Materiel Development and
Readiness Command
ATTN: DRCDR-DW, COL Collins
5001 Eisenhower Avenue
Alexandria, VA 22333

Commander
US Army Materiel Development and
Readiness Command
ATTN: DRCQA, Mr. R. Fahy
5001 Eisenhower Avenue
Alexandria, VA 22333

Commander
US Army Materiel Development and
Readiness Command
ATTN: DRCDMD
5001 Eisenhower Avenue
Alexandria, VA 22333

Commander
US Army Materiel Development and
Readiness Command
ATTN: DRCBSI
5001 Eisenhower Avenue
Alexandria, VA 22333

Commander
US Army Materiel Development and
Readiness Command
ATTN: DRCDMA-ST
5001 Eisenhower Avenue
Alexandria, VA 22333

Commander
US Army Materiel Development and
Readiness Command
ATTN: DRCSMA-ST, COL Vincent
5001 Eisenhower Avenue
Alexandria, VA 22333

Commander
US Army Materiel Development and
Readiness Command
ATTN: DRCSG, COL R. Cutting
5001 Eisenhower Avenue
Alexandria, VA 22333

Commander
US Army Materiel Development and
Readiness Command
ATTN: DRCPA-E, Mr. Pace
5001 Eisenhower Avenue
Alexandria, VA 22333

Commander
US Army Materiel Development and
Readiness Command
ATTN: DRCSG-R, LTC Bell
Washington, DC 20310

Commander
US Army Materiel Development and
Readiness Command
ATTN: DRCSF-P, Mr. Taras
5001 Eisenhower Avenue
Alexandria, VA 22333

Director
DARCOM Field Safety Activity
ATTN: DRXOS-ES, Mr. E. Olsen
Charlestown, IN 47111

Director
US Army Materiels and Mechanics
Research Center
ATTN: DRXMR-X, Dr. E. Wright
Watertown, MA 02172

Director
US Army Materiels and Mechanics
Research Center
ATTN: DRXMR-AR, Mr. S. Levin
Watertown, MA 02172

Director
US Army Materiels Systems
Analysis Agency
ATTN: DRXSY
Aberdeen Proving Ground, MD 21005

Director
US Army Materiels Systems Analysis
Agency
ATTN: DRXSY-GS, Mr. W. Brooks
Aberdeen Proving Ground, MD 21005

Director
US Army Materiels Systems Analysis
Agency
ATTN: DRXSY-GA, Mr. J. McCarthy
Aberdeen Proving Ground, MD 21005

Director
US Army Materiels Systems Analysis
Agency
ATTN: DRXSY-GA, Mr. R. Smith
Aberdeen Proving Ground, MD 21005

Commander
US Army Armament Materiel Readiness Cmd
ATTN: DRSAR-MAD-C, Mr. P. Shaw
Dover, NJ 07801

Commander
US Army Armament Materiel Readiness Cmd
ATTN: DRSAR-ASR, LTC Counihan
Rock Island, IL 61201

Commander
US Army Armament Materiel Readiness Cmd
ATTN: DRSAR-SF, Mr. B. Morris
Rock Island, IL 61201

Commander
US Army Armament Materiel Readiness Cmd
ATTN: DRSAR-CG
Rock Island, IL 61201

Commander
US Army Armament Materiel Readiness Cmd
ATTN: DRSAR-LEA, Mr. E. Beckman
Rock Island, IL 61201

Commander
US Army Armament Research and
Development Command
ATTN: DRDAR-CG, MG A. Light
Dover, NJ 07801

Commander
US Army Armament Research and
Development Command
ATTN: DRDAR-TD, Dr. R. Weigle
Dover, NJ 07801

Commander
US Army Armament Research and
Development Command
ATTN: DRDAR-BL, Dr. Eichelberger
Dover, NJ 07801

Commander
US Army Armament Research and
Development Command
ATTN: DRDAR-SC, Dr. D. Gyorog
Dover, NJ 07801

Commander
US Army Armament Research and
Development Command
ATTN: DRDAR-SCM, Mr. J. Corrie
Dover, NJ 07801

Commander
US Army Armament Research and
Development Command
ATTN: DRDAR-SCM, Dr. E. Bloore (10 cys)
Dover, NJ 07801

Commander
US Army Armament Research and
Development Command
ATTN: DRDAR-LCU-D-T, Mr. Davitt
Dover, NJ 07801

Commander
US Army Armament Research and
Development Command
ATTN: DRDAR-SF, Mr. Elliott
Dover, NJ 07801

Commander
US Army Armament Research and
Development Command
ATTN: DRDAR-BLT, Mr. R. Vitali
Aberdeen Proving Ground, MD 21005

Commander
US Army Armament Research and
Development Command
ATTN: DRDAR-BLT, Dr. W. Gillich
Aberdeen Proving Ground, MD 21005

Commander
US Army Armament Research and
Development Command
ATTN: DRDAR-BLV, Mr. E. Wilsey
Aberdeen Proving Ground, MD 21005

Commander
US Army Armament Research and
Development Command
ATTN: DRDAR-BLP, Mr. R. Comer
Aberdeen Proving Ground, MD 21005

Commander
US Army Armament Research and
Development Command
ATTN: DRDAR-AD-SA, Mr. Markland
Aberdeen Proving Ground, MD 21005

Commander
US Army Armament Research and
Development Command
ATTN: DRDAR-LCB, Mr. P. Rummel
Watervliet, NY 12189

Commander
US Army Mobility Equipment Research
and Development Command
ATTN: DRDME-RZT, Tech Doc Ctr B/315
Fort Belvoir, VA 22060

Commander
US Army Mobility Equipment
Research and Development Command
ATTN: DRDME-VR, Mr. McMillan
Fort Belvoir, VA 22060

Commander
US Army Combined Arms Combat
Development Activity
ATTN: APCA-BC
Fort Leavenworth, KA 66027

Commander
US Army Environment Hygience Agency
ATTN: HSE-O
Aberdeen Proving Ground, MD 21005

Director
US Army Human Engineering Laboratory
ATTN: DRXHE-HE, Mr. Erickson
Aberdeen Proving Ground, MD 23801

Commander
US Army Logistics Center
ATTN: ATCL-M, Mr. Thompson
Fort Lee, VA 23801

Commander
US Army Missile Munitions
ATTN: ATSK-CD
Redstone Arsenal, Alabama 35809

Commander
US Army Logistics Evaluation Agency
ATTN: DALO-LEI, Mr. Frye
New Cumberland Army Depot
New Cumberland, PA 17070

Director
US Army Ammunition Center
ATTN: SARAC-D, Mr. K. Croscost
Savanna, IL 61074

Commander
US Army Missile Command
ATTN: DRCPM-LCE, Mr. Crosswhite
Redstone Arsenal, AL 35809

Commander
US Army Research Office
ATTN: Dr. G. Mayer
PO Box 12211
Research Triangle Park, NC 27709

Commander
US Army Research Office
ATTN: Dr. E. Saibel
PO Box 12211
Research Triangle Park, NC 27709

Commander
US Army Tank Automotive Research
and Development Command
ATTN: DRDTA-RWL
Warren, MI 48090

Commander
US Army Tank Automotive Research
and Development Command
ATTN: DRDTA-RKA, Mr. V. Pagano
Warren, MI 48090

Commander
US Army Test and Evaluation Command
ATTN: DRSTE
Aberdeen Proving Ground, MD 21005

Commander
US Army Test and Evaluation Command
ATTN: DRSTE-AR, Mr. Brown
Aberdeen Proving Ground, MD 21005

Commander
US Army Test and Evaluation Command
ATTN: DRSTE-AR, Mr. Brown
Aberdeen Proving Ground, MD 21005

Commander
US Army Test and Evaluation Command
ATTN: DRSTE-CE
Aberdeen Proving Ground, MD 21005

Commander
US Army Test and Evaluation Command
ATTN: DRSTE-PP-E
Aberdeen Proving Ground, MD 21005

Commander
US Army Test and Evaluation Command
ATTN: DRSTE-ST, Mr. J. Starkey
Aberdeen Proving Ground, MD 21005

Commander
US Army Training and Doctrine Cmd
Fort Monroe
Hampton, VA 23651

Director
US Army TRADOC Systems Analysis Act
ATTN: ATAA-SA
White Sands Missile Range, NM 88002

Commander
US Army Foreign Science and Tech Ctr
ATTN: DRXST-CB, J. Bollendorf
7th Street, NE-Building 220
Charlottesville, VA 22901

Commander
Naval Facilities Engineering Cmd
Code 04N2, Mr. G. Hendrix
200 Stovall Street
Alexandria, VA 22333 (2 cys)

Commander
US Naval Ordnance Systems Command
ATTN: ORD-9132
Washington, DC 20360

Superintendent
US Naval Post Graduate School
ATTN: Director of Library
Monterey, CA 09340

Commander
Naval Sea Systems Command
ATTN: PMS-404-31, Mr. E. Gerlach
Washington, DC 20362

Commander
US Naval Surface Weapons Center
ATTN: Code WR-32, Dr. S. Fishman
White Oak, MD 20910

Commander
US Naval Surface Weapons Center
ATTN: Code DG-52, W. Wishard
White Oak, MD 20910

Commander
US Marine Corps Liaison Officer
Aberdeen Proving Ground, MD 21005

Commander
US Air Force Headquarters
ATTN: SG-PA, LTC J. Bayer
Washington, DC 20314

HQ ADTC/SCV
ATTN: MAJ R. Conrad
Eglin AFB, FL 32542

HQ ADTC/DLV
ATTN: Dr. J. Cornette
Eglin AFB, FL 32542

Commander
US Air Force Tactical Air Command
ATTN: SG-PA, LTC J. Coughlin
Langley AFB, VA 23665

National Lead Company of Ohio
ATTN: Mr. L. Levy
Box 39158
Cincinnati, OH 45239

Rockwell International
Rocky Flats Plant
ATTN: Mr. T. Crites
Bldg. 123, PO Box 464
Golden, CO 80401

The Analytic Sciences Corporation
ATTN: Dr. S. Bucci
Six Jacob Way
Reading, MA 01867

Union Carbide Corporation
Nuclear Division
ATTN: Mr. M. Sanders
PO Box Y
Oak Ridge, TN 37830

Nuclear Regulatory Commission
Division of Fuel Cycle and Material Safety
ATTN: Mr. E. Wright
Washington, DC 21055

University of California
Los Alamos Scientific Laboratory
ATTN: Dr. D. Sandstrom, CMB-6
Los Alamos, NM 87545

Air Force Materiel Laboratory
ATTN: LTM. S. Inouye
Wright-Patterson AFB, OH 45433

Air Force Materiel Laboratory
ATTN: XYD, CPT D. Schuur
Wright-Patterson AFB, OH 45433

HQ, ADTC
ATTN: CEEDO/CC Detachment 1
Tyndall AFB, FL 32403

USA Ordnance Center and School
Aberdeen Proving Ground, MD 21005

Battelle Northwest Laboratories
ATTN: Mr. R. Gilchrist
Battelle Blvd.
Richland, WA 99352

Director
DARCOM Field Safety Activity
ATTN: DRXOS-ES, Mr. L. Foley
Charlestown, IN 47111

☆U.S. GOVERNMENT PRINTING OFFICE: 1980—777-022/218

Printed in the United States of America
Available from
National Technical Information Service
US Department of Commerce
5285 Port Royal Road
Springfield, VA 22161

Microfiche $3.50 (A01)

Page Range	Domestic Price	NTIS Price Code	Page Range	Domestic Price	NTIS Price Code	Page Range	Domestic Price	NTIS Price Code	Page Range	Domestic Price	NTIS Price Code
001-025	$ 5.00	A02	151-175	$11.00	A08	301-325	$17.00	A14	451-475	$23.00	A20
026-050	6.00	A03	176-200	12.00	A09	326-350	18.00	A15	476-500	24.00	A21
051-075	7.00	A04	201-225	13.00	A10	351-375	19.00	A16	501-525	25.00	A22
076-100	8.00	A05	226-250	14.00	A11	376-400	20.00	A17	526-550	26.00	A23
101-125	9.00	A06	251-275	15.00	A12	401-425	21.00	A18	551-575	27.00	A24
126-150	10.00	A07	276-300	16.00	A13	426-450	22.00	A19	576-600	28.00	A25
									601-up	†	A99

†Add $1.00 for each additional 25-page increment or portion thereof from 601 pages up.